LA-UR-08-2219

Approved for public release; distribution is unlimited.

Title: Cross-sections for nuclide production in 56Fe target irradiated by 300, 500, 750, 1000, 1500, and 2600 MeV protons compared with data on hydrogen target irradiation by 300, 500, 750, 1000, and 1500 MeV/nucleon 56Fe ions

Author(s): Yu. E. Titarenko, V. F. Batyaev, A. Yu. Titarenko, M. A. Butko, K. V. Pavlov, S. N. Florya, R. S. Tikhonov, S. G. Mashnik, A. V. Ignatyuk, N. N. Titarenko, W. Gudowski, M. Tesinsky, C.-M. L. Persson, H. Ait Abderrahim, H. Kumawat, and H. Duarte

Submitted to: Physical Review C 78, 034615 (2008); E-print: arXiv:0804.1260

Cross sections for nuclide production in a ^{56}Fe target irradiated by 300, 500, 750, 1000, 1500, and 2600 MeV protons compared with data on a hydrogen target irradiated by 300, 500, 750, 1000, and 1500 MeV/nucleon ^{56}Fe ions

Yu. E. Titarenko,[1,*] V. F. Batyaev,[1] A. Yu. Titarenko,[1] M. A. Butko,[1] K. V. Pavlov,[1] S. N. Florya,[1] R. S. Tikhonov,[1] S. G. Mashnik,[2] A. V. Ignatyuk,[3] N. N. Titarenko,[3] W. Gudowski,[4] M. Těšínský,[4] C.-M. L. Persson,[4] H. Ait Abderrahim,[5] H. Kumawat,[6] and H. Duarte[7]

[1]*Institute for Theoretical and Experimental Physics (ITEP), RU-117218 Moscow, Russia*
[2]*Los Alamos National Laboratory, Los Alamos, New Mexico 87545, USA*
[3]*Institute for Physics and Power Engineering, RU-249020 Obninsk, Russia*
[4]*Royal Institute of Technology, S-106 91 Stockholm, Sweden*
[5]*Centre d'étude de l'énergie nucléaire, 200, Boeretang, Mol, B-2400 Belgium*
[6]*Bhabha Atomic Research Center, Mumbai-400085, India*
[7]*CEA/DIF, BP 12, F-91680 Bruyères-le-Châtel, France*

(Received 31 January 2008; revised manuscript received 7 April 2008; published 30 September 2008)

This work presents the cross sections for radioactive nuclide production in ^{56}Fe(p, x) reactions determined in six experiments using 300, 500, 750, 1000, 1500, and 2600 MeV protons of the external beam from the ITEP U-10 proton accelerator. In total, 221 independent and cumulative yields of radioactive residuals of half-lives from 6.6 min to 312 d have been obtained. The radioactive product nuclide yields were determined by direct γ-spectrometry. The measured data have been compared with the experimental data obtained elsewhere by the direct and inverse kinematics methods and with calculation results of 15 different codes that simulated hadron-nucleus interactions: MCNPX (INCL, CEM2K, BERTINI, ISABEL), LAHET (BERTINI, ISABEL), CEM03 (.01, .G1, .S1), LAQGSM03 (.01, .G1, .S1), CASCADE-2004, LAHETO, and BRIEFF. Most of the data obtained here are in a good agreement with the inverse kinematics results and disprove the results of some earlier activation measurements that were quite different from the inverse kinematics measurements. The most significant calculation-to-experiment differences are observed in the yields of the $A < 30$ light nuclei, indicating that further improvements in nuclear reaction models are needed, and pointing out as well to a necessity of more complete experimental measurements of such reaction products.

DOI: 10.1103/PhysRevC.78.034615 PACS number(s): 25.40.Sc, 24.10.−i, 29.30.Kv, 29.85.−c

I. INTRODUCTION

Spallation reactions have been a subject of permanent interest for more than 40 years due to the production of them a wide variety of residual nuclei, on the one hand, and an application of them as intensive neutron sources for both the direct physical and technological researches, and the power accelerator-driven reactor systems, on the other hand [1]. Safety conditions connected with such neutron sources require a sufficiently accurate estimation of the production yields for a large amount of radioactive nuclides accumulated in the corresponding targets and surrounding structural materials. Natural iron is one of the most frequently used structural materials and its nuclear data can be especially important for designing nuclear equipment working under intensive irradiation.

The present-day EXFOR database contains 40 original works [2–5], which present mainly the cumulative production cross sections of the proton-induced reaction products in natural iron (^{54}Fe-5.845%; ^{56}Fe-91.754%; ^{57}Fe-2.119%; ^{58}Fe-0.282%). All the data have been obtained using the proton irradiation of thin iron targets ($p \rightarrow {}^{\text{nat}}_{26}$Fe) and the gamma-ray spectrometric analysis to identify the resulting reaction products [2–5].

Recently the precise measurements of the residual production yields for ^{56}Fe were performed by the inverse kinematics method [6–8]. In the cases of [7,8], the accelerated ^{56}Fe ions irradiated a hydrogen target ($^{56}_{26}\text{Fe} \rightarrow {}^{1}_{1}\text{H}$) and the yields were measured for the ion kinetic energies of 300, 500, 750, 1000, and 1500 MeV/nucleon using the fragment separator at GSI (Darmstadt).

A comparison of data obtained by different techniques, but at the same energies, is of special interest, because such data are extensively used to verify basic theoretical models included in various high-energy transport codes.

II. TECHNIQUES FOR EXPERIMENTAL DETERMINATION OF THE RESIDUAL PRODUCTION CROSS SECTIONS

A comprehensive description of the method used for the measurements of the yields or the production cross sections of radioactive products from the proton-induced reactions can be found in the works [9–13]. We will briefly discuss below some details of our technique important for the present experiment.

*Yury.Titarenko@itep.ru

A. Determination of the residual production rates

For a consistent estimation of uncertainties of measured cross sections the concept of independent and cumulative reaction rates [12,13] is usually introduced, which can be determined by the following relations:

$$R^{\text{ind}} = \sigma^{\text{ind}}(E) \cdot \Phi(E) \quad \text{and} \quad R^{\text{cum}} = \sigma^{\text{cum}}(E) \cdot \Phi(E), \quad (1)$$

where $\sigma^{\text{ind}}(E)$ and $\sigma^{\text{cum}}(E)$ are, respectively, the independent and cumulative cross sections of a nuclide production and $\Phi(E)$ is the proton flux density.

The accumulation of the reaction products during the proton beam irradiation and afterwards is described by the set of kinetic equations, the solution of which for the reaction rates depends on both the decay constants of the involved radioactive nuclei and the irradiation conditions. Analytical expressions for the reaction rates have been obtained for the case of two- and three-link decay chains. In the present experiment the yield of nuclides produced at the two-link decay chains only were measured and the corresponding expressions for the reaction rates can be written in the form

$$R_1^{\text{cum/ind}} = \frac{A_1}{N_T \cdot \eta_1 \cdot \varepsilon_1} \cdot \frac{1}{F_1} \quad (2)$$

$$R_1^{\text{cum/ind}} = \frac{A_2^{'}}{N_T \cdot \eta_2 \cdot \varepsilon_2 \cdot \nu_{12}} \cdot \frac{\lambda_2 - \lambda_1}{\lambda_2} \cdot \frac{1}{F_1}, \quad (3)$$

$$R_2^{\text{ind}} = \left(\frac{A_2^{''}}{F_2} + \frac{A_2^{'}}{F_1} \cdot \frac{\lambda_1}{\lambda_2} \right) \cdot \frac{1}{N_T \cdot \eta_2 \cdot \varepsilon_2}, \quad (4)$$

$$R_2^{\text{cum}} = R_2^{\text{ind}} + \nu_{12} \cdot R_1^{\text{cum/ind}} = \left(\frac{A_2^{'}}{F_1} + \frac{A_2^{''}}{F_2} \right) \cdot \frac{1}{N_T \cdot \eta_2 \cdot \varepsilon_2}, \quad (5)$$

where A_1, A_2', and A_2'' are the parameters determined by the least square fitting of the experimental decay curves of the nuclei, with subscripts 1 and 2 designating the mother and daughter nuclides, respectively; N_T is the number of nuclei in an irradiated sample; η_1 and η_2 are the γ-ray abundances; λ_1 and λ_2 are the decay constants; ε_1 and ε_2 are the absolute spectrometer efficiencies at γ-energies E_1 and E_2; ν is the branching factor, i.e., the probability for a mother nuclide to turn unto its daughter; F_1 and F_2 are functions to be calculated as $F_i = (1 - e^{-\lambda_i \cdot t_{\text{irr}}})$; t_{irr} is the irradiation time.

B. Determination of the mean proton flux density

The mean proton flux density $\Phi(E)$ was determined using the ^{27}Al$(p, x)^{22}$Na monitor reaction. Figure 1 compiles the experimental data of 30 works made from 1955 to 1997 in 25 MeV–3.0 GeV energy range. Out of the data presented, the data of but two works by Tobailem, 1981 ($E_P > 200$ MeV) and Steyn, 1990 ($E_P < 200$ MeV) were chosen for monitoring purposes. In cases where energies were not supported with experimental cross sections, they were calculated via linear interpolation of the cross section logarithms at the boundaries of the given range.

In this case, the time- and sample area-averaged density of proton flux and its error are calculated as

$$\widehat{\Phi} = \frac{R^{^{22}\text{Na}}}{\sigma^{^{22}\text{Na}}} \quad \frac{\Delta\widehat{\Phi}}{\widehat{\Phi}} = \sqrt{\left(\frac{\Delta R^{^{22}\text{Na}}}{R^{^{22}\text{Na}}} \right)^2 + \left(\frac{\Delta\sigma^{^{22}\text{Na}}}{\sigma^{^{22}\text{Na}}} \right)^2}, \quad (6)$$

where $R^{^{22}\text{Na}}$ is the ^{22}Na production rate and $\sigma^{^{22}\text{Na}}$ is the monitor-reaction cross section at a given energy. The analytical expression to calculate the ^{22}Na production rate is the same as Eq. (2).

C. Preparation of samples

The samples have the diameter of 10.5-mm and were prepared by pressing the ^{56}Fe-enriched fine-dispersed iron powder (^{54}Fe—0.3%, ^{56}Fe—99.5 ± 0.1%, ^{57}Fe—0.2%, ^{58}Fe < 0.05%). The Al monitors were cut off from a foil and pressed then into the same master form to provide identity of the parameters. The samples and the monitors were weighed. After that, each of the sample-Al interlayer-Al monitor sandwiches was sealed into a polyethylene package to preserve the sandwich geometry and was then directed to irradiation.

The impurities amounted to ∼0.091% in the iron powder and to ∼0.01% in the Al foil.

D. Irradiation of samples

The experimental samples were irradiated using the U-10 ITEP proton synchrotron. The synchrotron serves as a ring facility with the 25 MeV-proton energy injector and the highest accelerated proton energy of 9.3 GeV. The accelerated proton beam with a given energy (ranging from 40 to 9300 MeV) consists from four bunches of a ∼250 ns duration each and is directed from the synchrotron ring to the transport channel that provides proton extraction of a $\sim 2 \times 10^{11}$ proton/pulse intensity, an elliptic cross section with 10×15 mm axes, ∼1 μs total duration, and ∼15 pulse/min pulse repetition rate. The transport channel and its elements are described in detail in [13].

During irradiation runs, a polyethylene package with a sample sandwich therein was fixed with a scotch to the center of a 50×50 mm, 0.1 mm thick Al plate placed in a task-oriented holder perpendicularly to the proton beam. The selected geometry precludes ^{24}Na, ^{22}Na, and ^{7}Be produced at the Al monitor from accumulating in the sample. The monitor provides the total control of a proton beam intensity. Table I presents the parameters of the ^{56}Fe sample irradiation.

During the experiment, the beam parameters were on-line controlled using current transformer together with the task-oriented digital-control PC plate with a 2 ns time resolution. The digitized data were recorded to a 2 μs full sweep file (∼1000 values) used to calculate the amplitudes of each proton pulse. Such data are needed to allow in detail for the decay of nuclei under irradiation, which is especially important for the short-lived nuclides.

TABLE I. The ^{56}Fe target irradiation parameters.

Energy (GeV)	Mass of sample (g)	Mass of monitor (g)	Irradiation time (min)	Mean proton flux (p/(cm^2 s) $\times 10^{10}$)
0.3	0.2422	0.0480	35	5.23 ± 0.38
0.5	0.2447	0.0486	33	6.73 ± 0.48
0.75	0.2433	0.0499	30	7.45 ± 0.64
1.0	0.2429	0.0494	35	6.11 ± 0.46
1.5	0.2429	0.0485	36	4.44 ± 0.37
2.6	0.2000	0.1202	30	1.70 ± 0.15

E. Measurement and processing of the gamma-ray spectra

The reaction products in the irradiated samples and monitors were identified by measuring the typical discreet gamma-ray spectra of produced nuclei. For that purpose, the gamma-ray spectrometer based on a coaxial Ge-detector was used with a 1.8 keV energy resolution for the 1332 keV gamma-line of ^{60}Co. The admissible spectrometer parameters and measurement modes were determined in preliminary experiments, and they were strictly controlled under subsequent measurements. To reduce the spectrometer load during the initial gamma-spectrum measurements, an experimental sample irradiated was placed at a considerable distance over the detector surface.

The temperature stability, the cascade summation effects, the maximum spectrometer load, and the absolute distance-energy efficiency $\varepsilon(E, H)$ of gamma-ray detection were controlled. The technique for determining $\varepsilon(E, H)$ has been described in detail in Ref. [13], which presents the analytical expressions to calculate the latter for the gamma-ray energies from 90 keV to 2600 keV and the distance between 40 and 1240 mm.

The gamma-ray spectra were analyzed with the GENIE-2000 code. After automated packet processing the measured spectra, the code permits operating for each spectrum with the interactive fitting mode to additionally examine the results of tentative processing.

The processed spectra were merged into a single file to form an input file for the SIGMA code. The code plots the time variations in the selected gamma-line intensities and identifies the corresponding nuclides in accordance the NUDAT database and the additional gamma-ray transition schemes presented in Refs. [18–20]. For identified nuclides

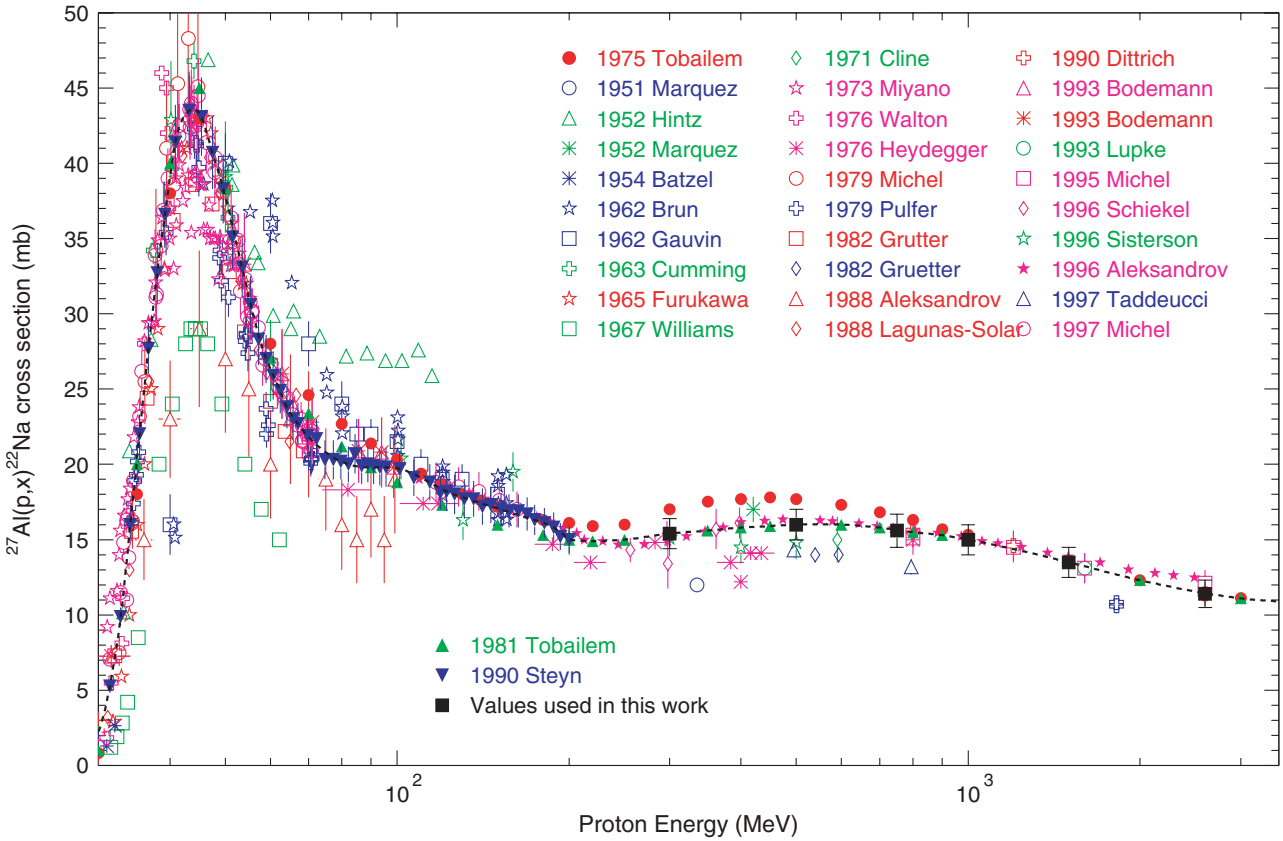

FIG. 1. (Color) The ^{27}Al(p, x) ^{22}Na reaction excitation function in the 25–3000 MeV proton energy range. Michel (1997)—[2], Michel (1995)—[2], Schiekel (1996)—[3], Cline (1971)—[5], Steyn (1990)—[14], Tobailem (1981)—[15], Tobailem (1975)—[16], Marquez (1951)—[17], Hintz (1952)—[17], Marquez (1952)—[17], Batzel (1954)—[17], Brun (1962)—[17], Gauvin (1962)—[17], Cumming (1963)—[17], Furukawa (1965)—[17], Williams (1967)—[17], Miyano (1973)—[17], Walton (1976)—[17], Heydegger (1976)—[17], Michel (1979)—[17], Pulfer (1979)—[17], Grutter (1982)—[17], Gruetter (1982)—[17], Aleksandrov (1988)—[17], Lagunas-Solar (1988)—[17], Dittrich (1990)—[17], Bodemann (1993)—[17], Bodemann (1993)—[17], Lupke (1993)—[17], Sisterson (1996)—[17], Aleksandrov (1996)—[17], Taddeucci (1997)—[17].

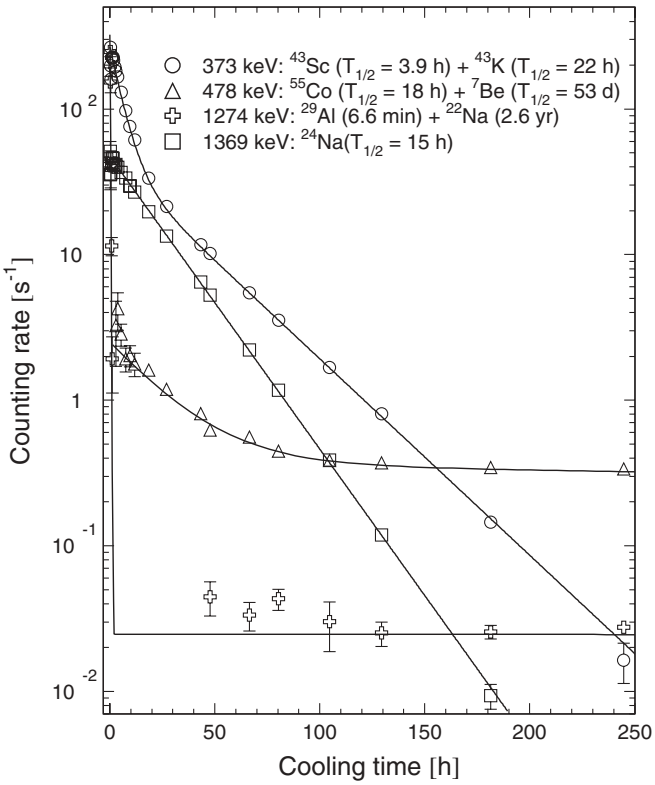

FIG. 2. Examples of the measured count rates and fitted decay curves.

the code calculates finally the nuclide production rate in accordance with the above formulas (2)–(5). Figure 2 shows some examples of the measured count rates versus cooling time, which are used for determining A_1, A_2', and A_2'' decay curve parameters of formulas (2)–(5), together fitted decay curves.

Table II presents the nuclear physics characteristics of nuclides produced in proton-irradiated ^{56}Fe used to identify the nuclides and to determine their cross sections.

III. EXPERIMENTAL RESULTS AND THEIR UNCERTAINTIES

Using formula (1), the production cross sections of independent and cumulative ^{56}Fe(p, x) reaction products and their uncertainties can be calculated to be

$$\sigma^{\text{ind/cum}} = \frac{R^{\text{ind/cum}}}{\widehat{\Phi}} \frac{\Delta\sigma^{\text{ind/cum}}}{\sigma^{\text{ind/cum}}} = \sqrt{\left(\frac{\Delta R^{\text{ind/cum}}}{R^{\text{ind/cum}}}\right)^2 + \left(\frac{\Delta\widehat{\Phi}}{\widehat{\Phi}}\right)^2} \qquad (7)$$

where $R^{\text{ind/cum}}$ is the ^{56}Fe(p, x) production rate, calculated via formulas (2)–(5); $\widehat{\Phi}$ is the mean proton flux density calculated by Eq. (6).

From our experiments, we have obtained 221 values of the residual production cross sections (yields) at various energies of incident protons, which include 54 independent yields (i), 18 independent yield for isomeric states of residual nuclides ($i(m)$), 17 sums of independent ground and isomeric states ($i(m + g)$), 132 cumulative and supracumulative yields (c, c^*). The supracumulative yield concept is discussed in Ref. [10]. Numerical values of obtained data are presented in Table III and plotted in Figs. 3–5.[1] For comparison, the figures present also the plots of other available data, as well as the results of cross section calculations with various codes discussed below.

As seen from Table II, a few gamma-lines were used instead a single one to estimate the reaction rates for more than a half of the measured cross sections. Therefore, a special method was developed to calculate the averaged rates. The respective analytical expressions are presented in [13].

The above technique is featured because the initial averaging step uses the relative yields m of different gamma-lines and the relative spectrometer efficiency at the energies of given gamma-lines, thereby permitting, according to formulas (2)–(5), the mean relative reaction rate to be calculated correctly. During the second step, the relative-to-absolute gamma-line yield transition coefficient is used together with the absolute activity of standard sources to determine the mean absolute production rate of each nuclide.

A. Analysis of errors

For an analysis of data obtained by different laboratories and comparison them with theoretical calculations it is necessary to take into consideration both the uncertainties of the measured reaction yields and the uncertainties of the incident proton energies.

The proton energy uncertainties arise from the U-10 synchrotron operations and from the geometric parameters of the transport channel that provides the 40–3000 MeV proton beam extraction. The constancy of proton orbit in a ring and the high accuracy ($\sim 10^{-2}$%) of determining the accelerating radio frequency requires in calculating the proton kinetic energy permit the energy error to be determined within ~0.5%.

The uncertainties in the reaction rates of residual nuclides produced in experimental sample and of ^{22}Na produced in Al monitor are due to the following two main factors. The first arises from the performances of the equipment used, from the γ-spectrometer operations, from the precision degree of the calibration gamma-ray sources, from the analytical balance accuracy, and from the certifying accuracy of the irradiated material compositions. The second factor is due to the uncertainties in the nuclear data from different databases and publications, namely, PCNUDAT [18], *Tables of Isotopes* (8th ed.) [19], ENSDF [20], photon cross section from 1 keV to 100 MeV for elements $Z = 1$ to $Z = 100$ [21], and the original works [the ^{27}Al(p, x) ^{22}Na monitor reaction cross sections] [22,23].

[1] Beside the data presented in Table III, Figs. 3–5 show the ^{56}Fe(p, x) reaction yields for 250, 400, 600, 800, 1200, and 1600 MeV proton energies as measured at ITEP under the current ISTC Project No. 3266. The complete numerical data will be presented in the final technical report on that project.

TABLE II. Nuclear physics characteristics of nuclides.

Nuclide	Half-life	Gamma-energies (E_γ, keV) and abundances (Y_γ, %)
^{57}Co	271.74 d	*122.1 (85.60), 136.5 (10.68)*
^{56}Co	77.233 d	*846.8 (99.94), 1037.8 (14.17), 1238.3 (66.9), 1360.2 (4.29), 1771.3 (15.47), 2015.2 (3.04), 2034.8 (7.89), 2598.5 (17.3)*
^{55}Co	17.53 h	*477.2 (20.2), 931.1 (75.0), 1408.5 (16.9)*
^{53}Fe	8.51 min	*377.9 (42.0)*
^{52}Fe	8.275 h	*168.7 (99.0)*
^{56}Mn	2.5789 h	*846.7 (98.), 1810.7 (27.2), 2113.1 (14.3)*
^{54}Mn	312.11 d	*834.8 (99.9760)*
^{52m}Mn	21.1 min	*1434.1 (99.8), 1727.5 (0.220)*
^{52}Mn	5.591 d	*744.2 (90.0), 848.2 (3.32), 935.5 (94.5), 1246.3 (4.21), 1333.7 (5.07), 1434.1 (100.0)*
^{51}Cr	27.7025 d	*320.1 (9.92)*
^{49}Cr	42.3 min	*90.6 (53.2), 152.9 (30.3)*
^{48}Cr	21.56 h	*112.3 (96.0), 308.2 (100.0)*
^{48}V	15.9735 d	*928.3 (0.77), 944.1(7.76), 983.5 (100.0), 1312.1 (97.5)*
^{48}Sc	43.67 h	*175.4 (7.48), 983.5 (100.1), 1037.5 (97.6), 1312.1 (100.1)*
^{47}Sc	3.3492 d	*159.4 (68.3)*
^{46}Sc	83.79 d	*889.3 (99.9840), 1120.5 (99.9870)*
^{44m}Sc	58.61 h	*270.9 (86.7), 1001.8 (1.20), 1126.1 (1.20)*
^{44}Sc	3.97 h	*1499.5 (0.908), 2656.5 (0.112)*
^{43}Sc	3.891 h	*372.8 (22.5)*
^{47}Ca	4.536 d	*1297.1 (71.0)*
^{44}K	22.13 min	*1499.4 (7.80), 2150.8 (23.0)*
^{43}K	22.3 h	*372.8 (86.80), 396.9 (11.85), 593.4 (11.26), 617.5 (79.2)*
^{42}K	12.360 h	*1525.0 (18.08)*
^{41}Ar	109.34 min	*1294 (99.10)*
^{39}Cl	55.6 min	*250.3 (46.3), 1267.0 (53.6), 1518.0 (39.2)*
^{38}Cl	37.24 min	*1643.0 (31.9), 2167.0 (42.4)*
^{34m}Cl	32.00 min	*146.4 (40.5), 1177.0 (14.09), 2127.0 (42.8)*
^{38}S	170.3 min	*1942.0 (83.0)*
^{29}Al	6.56 min	*1273.3 (90.6)*
^{28}Mg	20.915 h	*400.7 (36.6), 941.4 (38.3), 1342.3(52.6)*
^{27}Mg	9.458 min	*843.8 (71.8), 1014.4 (28.0)*
^{24}Na	14.9590 h	*1369.0 (100.0)*
^{22}Na	2.6019 yr	*1274.5 (99.944)*
^{7}Be	53.29 d	*477.6 (10.52)*

As shown by the calculations, the accuracy in experimentally determining the reaction rates is within 3.1%–95% (with 6.2% being the mean) and the accuracy of determining the mean proton flux is 7.1%–8.6%. Therefore, the accuracy of the above presented production cross sections (yields) of radioactive residuals is 7.8%–95%, with 10.7% being the mean. Figure 6 shows the distributions of the errors in reaction rates and cross sections.

The main uncertainties of formulas (2)–(6) contributors are as follows

(i) The statistical uncertainty of count rate in total absorption peak with due allowance for correction of unresolved γ-lines, of background under the peak, and γ-spectrum transients, as well as for the spectrometer dead time and count loss, to the total error of the nuclide production rate varies from 1.0% to 95%.

(ii) The uncertainty in the correction for γ-absorption in samples varies from 0.03% to 0.07%.

(iii) The uncertainty in the absolute spectrometer detection efficiency with due allowance for uncertainty in cascade summation effects and in contributions from the peaks of double and single ejections varies from 3.3% to 3.4%.

(iv) The contribution of the uncertainty in the γ-line abundance varies from 0% to 7.1%.

(v) The contribution of the uncertainty in the number of experimental sample nuclei is about 0.05%.

(vi) The ^{27}Al(p, x) ^{22}Na monitor reaction cross section uncertainty to the proton flux density uncertainty varies from 6.3% to 7.9%.

As shown by the above analysis, the main uncertainties are presented by statistical errors, absolute spectrometer detection efficiency, and γ-abundance uncertainty in the case of experimental samples, and by absolute spectrometer detection efficiency only in the case of monitors.

The uncertainty in the proton flux density arises from the monitor reaction uncertainty only.

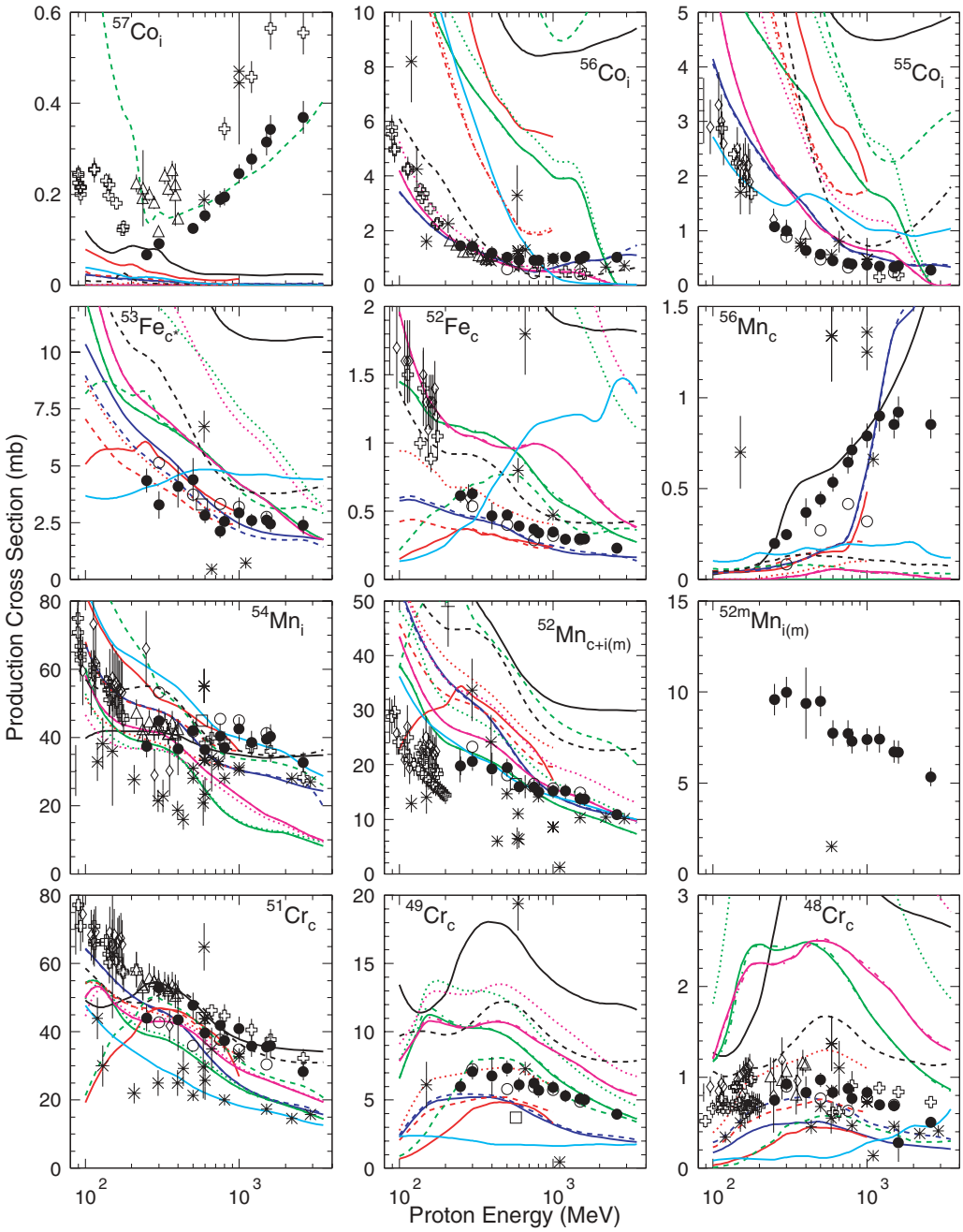

FIG. 3. (Color) ^{56}Fe(p, x) nuclide production cross sections measured at ITEP (●), GSI (○, [7]), R. Michel *et al.* (✣, [2]), Th. Shiekele *et al.* (△, [3]), M. Fassbender *et al.* (◇, [4]), W. R. Webber *et al.* (□, [6]), others (✳, [5]), compared with calculations by INCL/MCNPX (solid black), BRIEFF1.5.4g (dashed black), CEM03.01 (solid green), CEM2K/MCNPX (dashed green), CEM03.G1 (dotted green), CEM03.S1 (dashed-dotted green), BERTINI (MCNPX—solid blue, LAHET—dashed blue), ISABEL (MCNPX—solid red, LAHET—dashed red, LAHETO—dotted red), LAQGSM03.01 (solid magenta), LAQGSM03.G1 (dotted magenta), LAQGSM03.S1 (dashed-dotted magenta), CASCADE-2004 (cyan).

The uncertainties determined by the sample compositions, by the uncertainty in the correction that allows for the measured nuclide production from secondaries, by the decay constant uncertainties, and by the uncertainties in the irradiation, decay, and measurement times ($t_{\rm irr}$, t_d, t) were disregarded because of their smallness, which did not actually affect the uncertainties in the results.

B. Comparison with the data obtained elsewhere

We compare our current data with previous measurements from 42 works [2–8]. For convenience, we divide all data into seven groups and show them with different symbols in Figs. 3–5, respectively: Our current data presented in Table III are shown with filled circles; the GSI inverse kinematics data [7] are shown with open circles; the data

TABLE III. Experimental values of ^{56}Fe(p, x) product cross sections for E_P = 300, 500, 750, 1000, 1500, and 2600 MeV protons.

Product	Type	$T_{1/2}$	Cross section $\sigma \pm \Delta\sigma$ (m barn)					
			$E_P = 300$ MeV	$E_P = 500$ MeV	$E_P = 750$ MeV	$E_P = 1000$ MeV	$E_P = 1500$ MeV	$E_P = 2600$ MeV
^{57}Co	i	271.74 d	0.091 ± 0.008	0.125 ± 0.010	0.189 ± 0.018	0.245 ± 0.021	0.314 ± 0.029	0.369 ± 0.036
^{56}Co	i	77.233 d	1.42 ± 0.12	1.02 ± 0.08	0.908 ± 0.083	0.976 ± 0.080	0.960 ± 0.086	1.02 ± 0.10
^{55}Co	i	17.53 h	1.00 ± 0.08	0.570 ± 0.046	0.402 ± 0.041	0.375 ± 0.039	0.329 ± 0.030	0.276 ± 0.027
^{53}Fe	c^*	8.5 min	3.28 ± 0.60	4.39 ± 0.95	2.14 ± 0.33	2.93 ± 0.69	2.62 ± 0.32	2.39 ± 0.40
^{52}Fe	c	8.275 h	0.628 ± 0.050	0.471 ± 0.037	0.372 ± 0.034	0.349 ± 0.028	0.301 ± 0.027	0.230 ± 0.021
^{56}Mn	c	2.5789 h	0.246 ± 0.021	0.442 ± 0.044	0.644 ± 0.060	0.791 ± 0.066	0.852 ± 0.076	0.854 ± 0.079
^{54}Mn	i	312.11 d	44.9 ± 3.6	42.0 ± 3.3	40.4 ± 3.7	42.4 ± 3.5	39.4 ± 3.5	32.7 ± 3.0
^{52m}Mn	$i(m)$	21.1 min	9.98 ± 0.85	9.49 ± 0.83	7.71 ± 0.73	7.37 ± 0.64	6.72 ± 0.62	5.33 ± 0.51
^{52m}Mn	c	21.1 min	10.6 ± 0.9	9.97 ± 0.87	8.17 ± 0.82	7.76 ± 0.67	7.08 ± 0.69	5.55 ± 0.53
^{52}Mn	c	5.591 d	14.4 ± 1.2	12.0 ± 1.0	10.0 ± 0.9	9.63 ± 0.82	8.56 ± 0.78	6.80 ± 0.63
^{51}Cr	c	27.7025 d	52.9 ± 4.3	47.7 ± 3.8	41.9 ± 3.9	41.0 ± 3.4	35.5 ± 3.2	28.3 ± 2.6
^{49}Cr	c	42.3 min	7.08 ± 0.57	7.31 ± 0.58	6.26 ± 0.58	5.92 ± 0.49	5.09 ± 0.47	3.96 ± 0.37
^{48}Cr	c	21.56 h	0.929 ± 0.080	0.973 ± 0.078	0.875 ± 0.081	0.836 ± 0.070	0.690 ± 0.063	0.504 ± 0.047
^{48}V	c	15.9735 d	22.0 ± 1.8	23.0 ± 1.8	21.1 ± 1.9	20.6 ± 1.7	17.4 ± 1.5	13.3 ± 1.2
^{48}Sc	i	43.67 h	0.313 ± 0.039	0.473 ± 0.040	0.553 ± 0.053	0.607 ± 0.060	0.547 ± 0.055	0.437 ± 0.045
^{47}Sc	i	3.3492 d	2.32 ± 0.19	3.26 ± 0.26	3.58 ± 0.33	3.73 ± 0.31	3.40 ± 0.31	2.66 ± 0.24
^{47}Sc	c	3.3492 d	2.36 ± 0.19	3.30 ± 0.26	3.62 ± 0.34	3.80 ± 0.32	3.44 ± 0.31	2.71 ± 0.25
^{46}Sc	$i(m+g)$	83.79 d	6.93 ± 0.56	9.51 ± 0.75	10.2 ± 0.9	10.6 ± 0.9	9.33 ± 0.84	7.16 ± 0.67
^{44m}Sc	$i(m)$	58.61 h	5.58 ± 0.44	8.45 ± 0.66	9.46 ± 0.86	9.87 ± 0.80	8.94 ± 0.79	6.33 ± 0.57
^{44}Sc	$i(m+g)$	3.97 h	10.3 ± 1.5	15.9 ± 2.0	18.8 ± 4.0	18.9 ± 2.5	17.2 ± 1.8	12.8 ± 1.3
^{44}Sc	i	3.97 h	6.05 ± 0.63	9.6 ± 1.1	11.3 ± 1.9	11.1 ± 1.4	7.8 ± 1.2	6.69 ± 0.75
^{43}Sc	c	3.891 h	3.07 ± 0.27	5.14 ± 0.44	6.07 ± 0.59	6.49 ± 0.58	5.66 ± 0.54	4.08 ± 0.39
^{47}Ca	c	4.536 d	0.031 ± 0.002	0.032 ± 0.002	0.045 ± 0.004	0.058 ± 0.005	0.051 ± 0.005	0.053 ± 0.005
^{44}K	c^*	22.13 min	–	–	0.188 ± 0.080	0.254 ± 0.069	0.267 ± 0.067	0.383 ± 0.365
^{43}K	c	22.3 h	0.467 ± 0.037	0.962 ± 0.076	1.33 ± 0.12	1.53 ± 0.14	1.48 ± 0.13	1.16 ± 0.11
^{42}K	i	12.360 h	1.62 ± 0.13	3.28 ± 0.26	4.39 ± 0.41	5.08 ± 0.42	4.84 ± 0.44	3.89 ± 0.35
^{41}Ar	c	109.34 min	0.166 ± 0.014	0.416 ± 0.034	0.650 ± 0.060	0.809 ± 0.067	0.846 ± 0.076	0.699 ± 0.064
^{39}Cl	c	55.6 min	0.074 ± 0.010	0.227 ± 0.022	0.387 ± 0.037	0.500 ± 0.044	0.556 ± 0.053	0.519 ± 0.051
^{38}Cl	$i(m+g)$	37.24 min	0.263 ± 0.047	–	1.44 ± 0.14	1.95 ± 0.17	2.18 ± 0.20	1.67 ± 0.17
^{38}Cl	c	37.24 min	0.276 ± 0.028	0.913 ± 0.081	1.48 ± 0.14	1.99 ± 0.17	2.23 ± 0.21	1.71 ± 0.17
^{34m}Cl	$i(m)$	32.00 min	0.086 ± 0.013	0.287 ± 0.031	0.653 ± 0.063	0.903 ± 0.079	1.05 ± 0.10	0.871 ± 0.084
^{38}S	c	170.3 min	–	–	0.029 ± 0.003	0.046 ± 0.004	0.049 ± 0.004	0.046 ± 0.004
^{29}Al	c	6.56 min	–	0.363 ± 0.041	0.84 ± 0.12	1.61 ± 0.41	2.48 ± 0.26	1.59 ± 0.41
^{28}Mg	c	20.915 h	0.008 ± 0.001	0.048 ± 0.007	0.111 ± 0.011	0.209 ± 0.020	0.355 ± 0.034	0.392 ± 0.036
^{27}Mg	c	9.458 min	–	0.174 ± 0.022	0.463 ± 0.053	0.59 ± 0.11	1.30 ± 0.13	1.54 ± 0.16
^{24}Na	c	14.9590 h	0.072 ± 0.020	0.293 ± 0.034	0.977 ± 0.097	1.80 ± 0.16	3.05 ± 0.28	3.69 ± 0.34
^{22}Na	c	2.6019 yr	0.070 ± 0.014	0.264 ± 0.024	0.672 ± 0.064	1.35 ± 0.11	2.35 ± 0.21	3.20 ± 0.34
^{7}Be	i	53.29 d	0.891 ± 0.076	1.90 ± 0.16	3.19 ± 0.30	4.87 ± 0.40	7.30 ± 0.66	8.91 ± 0.82

by Michel *et al*. [2] are shown with open crosses; the data by Webber *et al*. [6] are shown with open squares; the data by Schiekel *et al*. [3] are shown with open triangles; the data by Fassbender *et al*. [4] are shown with open diamonds; the data from the rest of the 32 works [5] have been united into a single group and are shown with stars.

Using the procedure described below to calculate cumulative yields from independent ones, as well as the mean square deviation factor $\langle F \rangle$, which is usually employed to analyze various theoretical and experimental data, the current ITEP and GSI [7] data were compared quantitatively. The $\langle F \rangle$ values were calculated by formula

$$\langle F \rangle = 10^{\sqrt{\langle [\lg(\sigma_{\mathrm{cal}_i}/\sigma_{\mathrm{exp}_i})]^2 \rangle}}. \quad (8)$$

Within this approach, all products were divided into two groups of spallation ($A > 30$) and fragmentation ($A < 30$) products, respectively. Table IV presents the comparison results.

As the data from the rest of the works [2–8] have been obtained at different energies, we compare them with our results only qualitatively, in Figs. 3–5. Comparing our results with the data by Michel *et al*. [2], we can observe some serious discrepancies only for ^{57}Co at all energies, for ^{48}Cr at energies above 1 GeV, and for ^{52}Mn at energies below 200 MeV, while other cross sections agree reasonably well. With the data by Schiekel *et al*. [3], we see some big discrepancies only for ^{57}Co, and with the data by Fassbender *et al*. [4], only for ^{52}Mn.

TABLE IV. The mean square deviation factor $\langle F \rangle$ of the ITEP and GSI data for different incident proton energies and mass numbers of the products groups.

Product mass (A)	Proton energy (MeV)					All energies, all products
	300	500	750	1000	1500	
$A < 30$	3.14	1.67	1.33	1.25	1.14	
$A > 30$	1.34	1.28	1.28	1.28	1.25	1.34
All A	1.53	1.37	1.28	1.28	1.23	

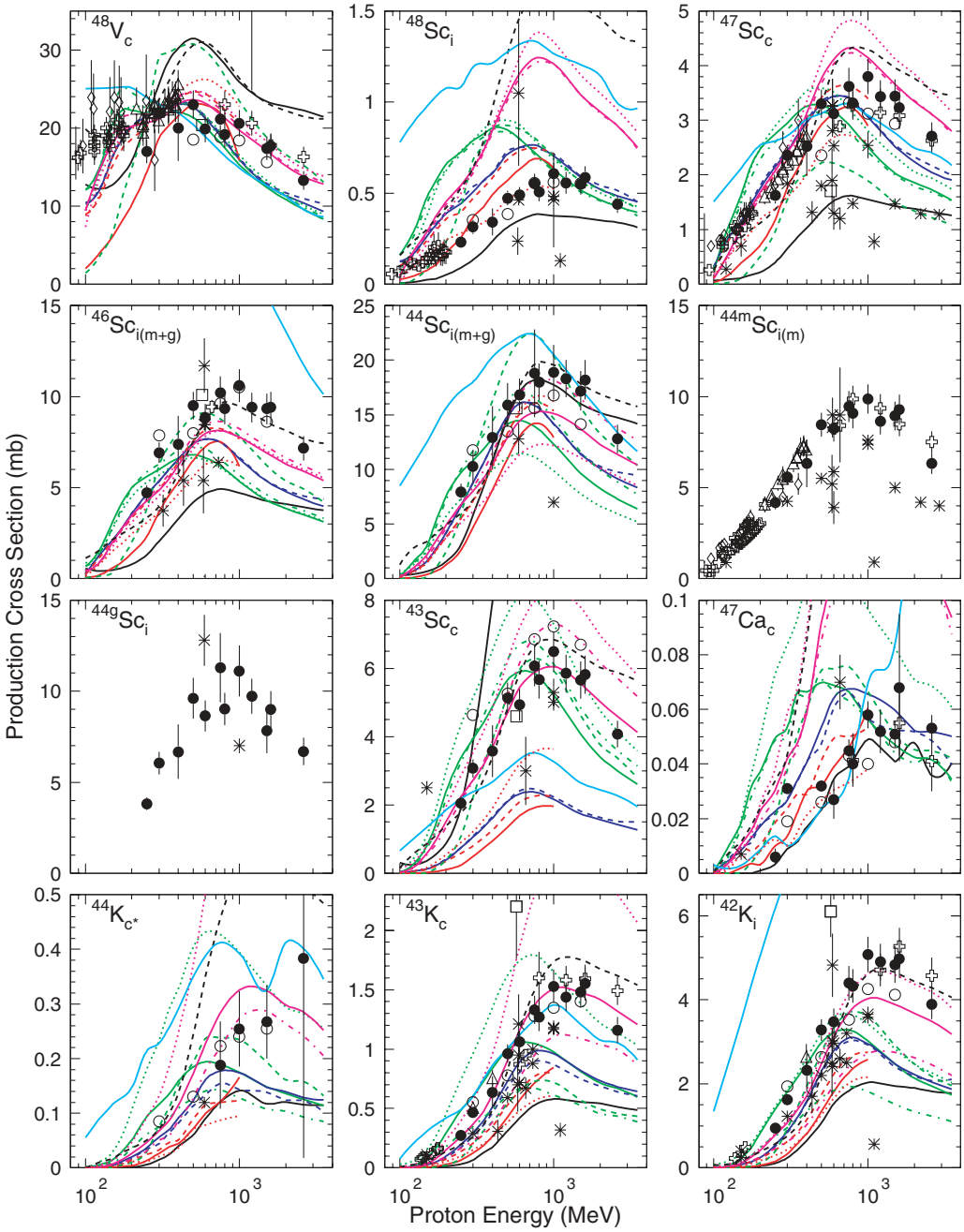

FIG. 4. (Color) Continuation of Fig. 3.

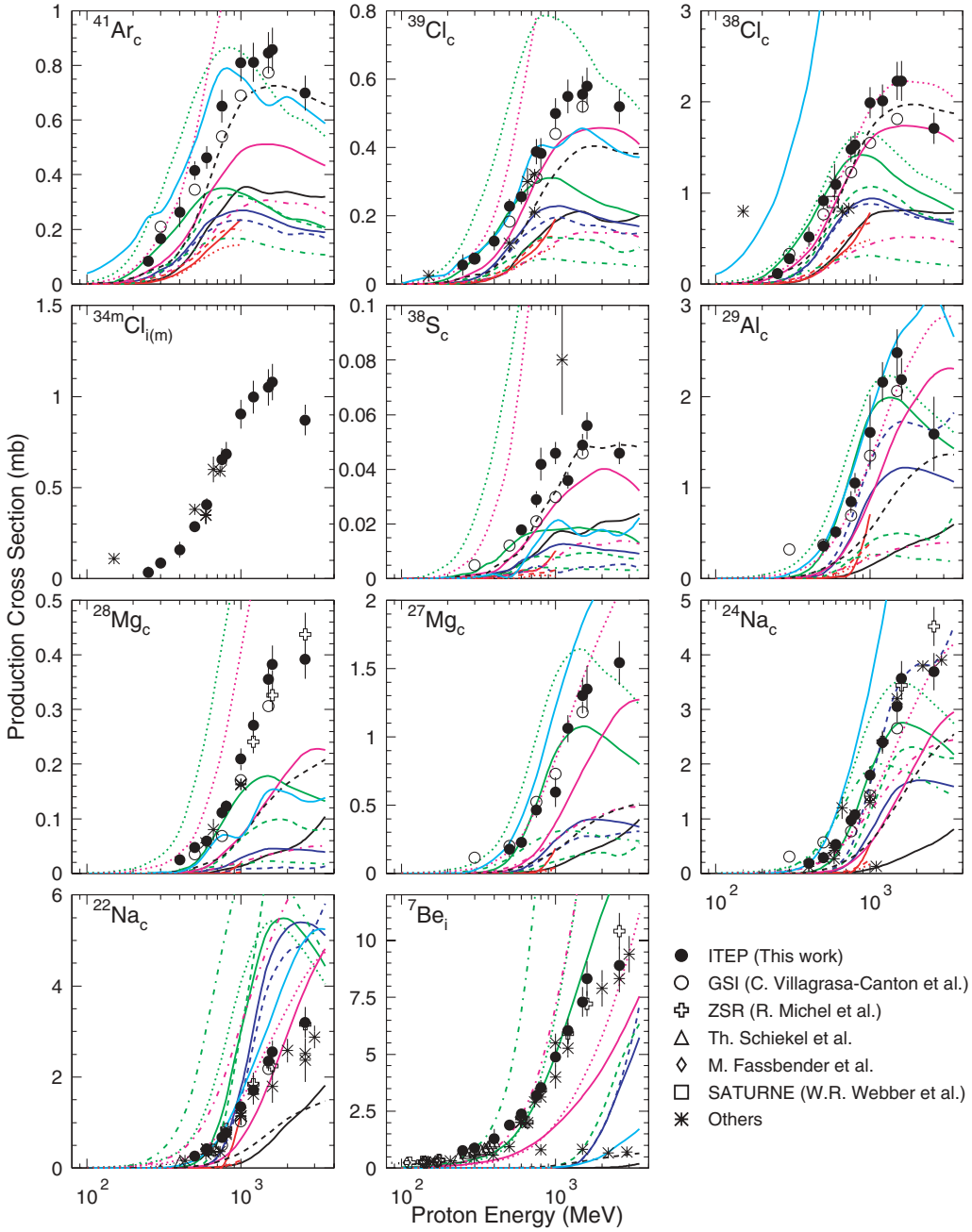

FIG. 5. (Color) Continuation of Fig. 4.

The discrepancy in the case of ^{57}Co with the data by Michel *et al.* is explained by the difference in the isotopic compositions of the irradiated samples: We used at ITEP enriched ^{56}Fe samples, while Michel *et al.* irradiated samples of natural iron, where ^{57}Co could be produced via ^{57}Fe$(p, \gamma n)^{57}$Co and ^{58}Fe$(p, \gamma 2n)^{57}$Co additional reactions not contributing in our case.

As to the comparison of our results with the inverse kinematics data of Webber *et al.* [6], it is of importance to note that the data of [6] on ^{42}K and ^{43}K are overestimated about two-fold compared with both our data and the data obtained elsewhere, the GSI data [7] in particular. It may be admitted, therefore, that the notable differences (up to a factor of 3) between the data of [6] and [7] presented in Fig. 12 of [7] must be interpreted to be significant systematic overestimations in [6].

The discrepancies in other cases have arisen from the different databases used, from different monitor reaction cross sections, and from differences in the methods for determining the absolute and relative spectrometer detection efficiencies.

The comparison quality deteriorates also because the short-lived nuclides with $T_{1/2} < 4$ h were not compared, as the relevant data are not presented in other works.

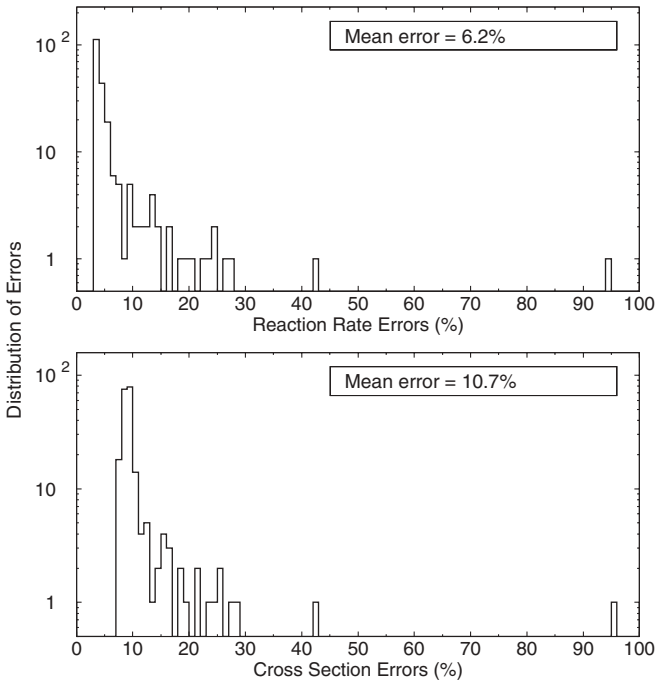

FIG. 6. Distributions of the errors in reaction rates (top plot) and in cross sections (bottom plot).

IV. CALCULATIONS OF CUMULATIVE CROSS SECTIONS FROM INDEPENDENT ONES

As a rule, theoretical models provide the production cross section of each nuclide independently from the possible following decay of the nuclide. Just the same cross sections, named usually as independent ones, are measured by the GSI inverse-kinematics method. On the other hand, measurements by the activation method correspond at most cases to the cumulative yields of nuclides produced after a chain of successive β-decays. To compare the data of activation measurements with the GSI data or theoretical model results the cumulative cross sections should be evaluated from the available independent cross sections. The procedure of calculating the cumulative and reduced cumulative yields is described in detail in [13], therefore we recall here only the main ideas. If the radioactive nuclide transformation chain is presented as shown in Fig. 7, then the cumulative cross sections can be estimated by the following expression:

$$\vec{\sigma}^{\,\mathrm{cum}} = M \cdot \vec{\sigma}^{\,\mathrm{ind}}, \tag{9}$$

where M is a matrix with elements m_{kj}; $\vec{\sigma}^{\,\mathrm{cum}}$ and $\vec{\sigma}^{\,\mathrm{ind}}$ are the vectors, whose elements are the cumulative and independent cross sections of chain elements, respectively.

The matrix elements m_{kj} can be calculated as

$$m_{kj} = \begin{cases} \sum_{i=j}^{k-1} \nu_{ik} \cdot m_{ik}, & \text{for} \quad k > j, \\ 1, & \text{for} \quad k = j,. \\ 0, & \text{for} \quad k < j, \end{cases} \tag{10}$$

where ν_{ik} are the branching factors, which determine the probability of the ith nuclide to be transformed into the kth nuclide. The branching factors ν_{ik} can be retrieved from the ENSDF database [20] that includes up to 18 modes of radioactive decays: β^-, $\beta^- n$, IT, ε, $\varepsilon + \beta^+$, p, α, $\beta^+ p$, $\beta^+\alpha$, $\beta^+ 2p$, εp, $\varepsilon\alpha$, 2ε, n, β^+, $2\beta^+$, $2\beta^-$, $2|e$.

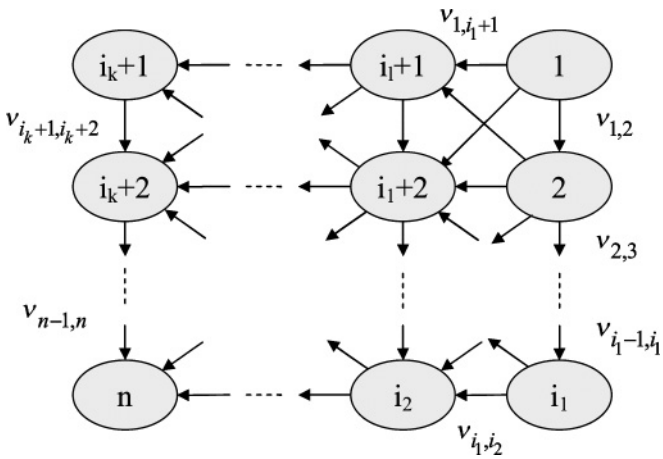

FIG. 7. The radioactive transformation diagram.

V. THEORETICAL SIMULATIONS WITH VARIOUS CODES

The obtained experimental data were analyzed with 15 different codes, which consider the nuclear reactions at high energies as three-stage processes: the intranuclear cascade (INC) of high-energy nucleon collisions followed by the preequilibrium emission of particles with intermediate energies and finally the successive evaporation of low-energy particles from compound nucleus or nuclear fission, if the compound nucleus is heavy enough for fission. The codes used in the present analysis were the LAHET complex [24] with both BERTINI [25] and ISABEL [26] options of INC; the MCNPX complex [27] that includes both LAHET options and also two additional code-systems: the CEM2K code with its own models for all three stages [28] and the Liège INCL4 code [29] merged with the GSI evaporation model ABLA [30]. Beside these six codes also used were the upgraded versions of the JINR CASCADE code [31], the Obninsk modification of the LAHET code [32], the Bruyères-le-Châtel BRIEFF complex [33,34], and the recent LANL complex of the CEM03 and LAQGSM03 codes [35,36]. A brief discussion of the models included in the above codes is presented below.

A. LAHET

This code system was widely used during almost two decades for the transport calculations of the high-energy particle interaction with composite targets of a rather complex geometry [24]. It was originally developed as the High Energy Transport Code (HETC) at ORNL [37] and was essentially modified latter at LANL [24]. Due to many new features added at LANL the modified code has been renamed as LAHET and its current versions enable to analyze interaction of nucleons, pions, muons, antinucleons, and light ions with atomic nuclei and any composite materials.

LAHET contains the Bertini INC model [25] to describe nucleon-nucleus interactions below 3.5 GeV and a scaling approximation to extend the energy region to arbitrary high energies, although a reasonable upper limit is about 10 GeV. As an alternative to the Bertini INC, LAHET also includes the ISABEL INC code [26] that is preferable for the incident particle energies below 1 GeV/nucleon.

LAHET considers preequilibrium processes as an intermediate stage between the intranuclear cascade and the evaporation/fission stage [38] and calculates multiple emissions of n, p, d, t, ^{3}He, and ^{4}He for both stages. When the excited nucleus produced after the preequilibrium stage has a mass number lower than 18, LAHET uses the Fermi breakup model [39–42] instead of the standard evaporation model to describe the decay of light nuclei. In the current version of LAHET, only two- and three-body breakup channels are included in spite of a larger number of decay channels considered by the previous breakup calculations on light nuclei [43].

LAHET includes two models for nuclear fission: the Atchison RAL fission-model [44] and the ORNL version [45] based on the Fong fission model [46]. Because iron is a light enough nucleus its fission probability is extremely low in these models and it was neglected at the following calculations.

B. MCNPX

MCNPX is a next generation of the high-energy transport codes developed at Los Alamos [27,47]. Its development started in 1994 on purpose to simplify the LAHET applications, to extend the interaction models for high-energy physics, and to provide high-energy calculations with the capabilities of the LANL low-energy transport code MCNP.

Initially, only the LAHET models discussed above were included into MCNPX. However, two alternative models were added to the later MCNPX versions: the CEM2K code based on the cascade exciton model (CEM) developed initially at JINR, Dubna [48] and the Liège INCL4 code by Cugnon *et al.* [29] merged with the GSI evaporation model ABLA [30]. The following features of the added codes should be mentioned:

(i) CEM2K is an improved version of the CEM95 and CEM97 codes described in details in Refs. [49,50]. Physical models included in the codes are similar as for LAHET, but the concrete realization of INC, preequilibrium, and evaporation models differs in many respects. In particular, the preequilibrium model of CEM takes into account all possible particle-hole transitions, while the LAHET model considers only transitions to more complex particle-hole states (the "never-come-back" approximation). There are also some essential differences between the angular distribution descriptions of emitted particles for the INC and preequilibrium stages. (ii) INCL4 is the latest version of the Liège INC model developed under the HINDAS project [29] and combined all previous model modifications [51–56]. The main improvements of INCL4 relate to an introduction of a smooth nuclear surface, a more consistent implementation of the Pauli blocking principle, and using a much longer stopping time for INC than in previous versions. As result of a long stopping time the intermediate stage of relatively slow intranuclear cascade collisions, which is considered as a preequilibrium one by LAHET, CEM, and many other codes, is described by INCL4 still as the cascade continuation that is followed by the final evaporation stage. Different evaporation codes were tested in a conjunction with INCL4 and the final preference was given to the ABLA code developed at GSI [30].

It should be noted that MCNPX uses more recent and updated values for nuclear masses and binding energies, due to which the MCNPX calculations can differ slightly from the results obtained with the original LAHET, CEM, or INCL4 codes. For similar reasons small differences can exist between the calculations with various MCNPX versions. The calculations presented below were performed with the version MCNPX-2.5.0.

C. CASCADE-2004

CASCADE-2004 [31] is an upgrade of the CASCADE code [57–60] developed at JINR, Dubna to simulate reactions on both thin and thick targets. The INC is described with an old version of the dubna cascade model (DCM) [61] simulating reactions induced by both particles and nuclei. The preequilibrium stage of reactions is described by the modified exciton model (MEM) [62,63], as realized in the code CEM95 [50]. The evaporation stage of the code was written at JINR (see [58] and references therein) and is based on the Dostrovsky *et al.* model [64]. The main difference between CASCADE-2004 and its precursor versions relates to an improved description of the evaporation stage that was developed at JINR by Kumawat [31,65].

D. LAHETO

LAHETO [32] is an upgraded and modified version of LAHET used at IPPE, Obninsk. It was developed only for the ISABEL option [26], therefore we do not use it here at incident energies above 1 GeV. In LAHETO, modifications and improvements were made in comparison with LAHET to all three stages of reactions, namely:

(i) At the INC stage, corrections were made for nucleon-nucleon and pion-nucleon elementary cross sections to describe better the available experimental data. Actually, the updated elementary cross sections for such interactions from CEM2K [28] were incorporated into LAHETO;
(ii) At the preequilibrium stage, improved values for the Coulomb radius parameters were incorporated into the Obninsk version to calculate the charge particle widths;
(iii) Finally, the evaporation and fission models of LAHET were modified taking advantage of the IPPE experience on the level density analysis (see [66,67] and references therein).

E. BRIEFF1.5.4g

BRIEFF is a code developed at CEA, Bruyères-le-Châtel [33,34]. It is composed of the INC code BRIC [33], of the evaporation code based on the statistical theory of Weisskopf and Ewing [68], of the modified Fermi breakup model [42], and of the Atchison fission model (the RAL code) [44] slightly modified to be consistent with the evaporation stage.

The INC code BRIC uses a time-dependent approach similar to the Liège INC model. In comparison to the original version [69], the code has been essentially improved for intermediate energies by using the realistic equations of the particle motion inside a nucleus and the in-medium nucleon-nucleon cross sections [33,70]. These modifications should guarantee that the final steps of INC simulate rather reasonably the preequilibrium stage of nuclear processes. With the same purpose there were estimated more precisely the initialized conditions of hadron-nucleus collisions and the energy distributions of collision products for later steps of the cascade [34].

The essential modifications were also made for the reaction cross sections used for the evaporation stage. Calculations of the partial widths of evaporated particles ($p, n, d, t,{}^3$He, and ^{4}He) require the cross sections of a compound-nucleus formation. While in previous versions such cross sections were estimated on the basis of the Glauber model for all charged particles and a combination of the Glauber model with the low-energy optical-model calculations for neutrons, for the current version of BRIEFF 1.5.4G the cross sections of a compound-nucleus formation were calculated directly with the BRIC INC for about 3300 target nuclei. Such an approach allows removing from the reaction cross sections a contribution related to the preequilibrium processes [34]. For deuterons, tritons and helium-particles the required cross sections were obtained renormalizing the previous reaction cross sections to the ratio of the new and previous ones for protons and their threshold energies taken from the BRIC code. Calculations of the partial widths require also the nuclear level densities that were evaluated on the basis of the back-shifted Fermi-gas model or the energy-dependent level density parameter model by Ignatyuk *et al.* [66].

The Fermi breakup model replaces the evaporation model when masses of compound nuclei after INC or during the evaporation stage are less than 30.

F. CEM03 and LAQGSM03

CEM03 and LAQGSM03 are the recent versions of the cascade-exciton model and of the Los Alamos version of the quark-gluon string model (LAQGSM) [35,36]. There are three code versions for each model, which differ by the additional reaction modes included into the codes. The basic versions CEM03.01 and LAQGSM03.01 consider only the traditional stages of nuclear reactions: INC, the preequilibrium processes, and all forms of the successive particle evaporation or fission, as described by a modification of the generalized evaporation model code GEM2 by Furihata [71].

The CEM03.S1 and LAQGSM03.S1 versions include additionally the multifragmentation processes for excited nuclei produced after the preequilibrium stage with the excitation energy above 2A MeV. The statistical multifragmentation model (SMM) by Botvina *et al.* [72–76] is used to simulate such processes (the extension "S" corresponds to SMM). A total accessible phase space determines the decay probabilities of all possible reaction products in this model, and its detailed description together with a large amount of results obtained for many reactions may be found in Refs. [72–76]. The corresponding SMM code was combined with CEM03 and LAQGSM03 without modifications.

The CEM03.G1 and LAQGSM03.G1 use the binary-decay GEMINI code [77–81], which realized the asymmetry-fission Moretto model [82] instead of using GEM2 [71]. The extension "G" corresponds to GEMINI in this case. The emission of the lightest particles, from neutron and proton up to beryllium isotopes, is calculated in such an approach on the basis of the Hauser-Fashbach formalism, but the yields of heavier reaction products are simulated by means of the transition-state decay probabilities of asymmetric fission-like configurations. GEMINI is described in details in Refs. [77–82] and the corresponding code was combined with CEM03 and LAQGSM03.

Improvements of CEM03.01 relative to CEM2K connected mainly with a revision of elementary cross sections, which were updated on the basis of currently available experimental data [83,84]. New algorithms were developed for a parametrization of the cross sections, for the extrapolation of them to higher energies and for a simulation of angular and energy distribution of particles produced in nucleon-nucleon, pion-nucleon, and photon-nucleon collisions.

Some modifications were introduced also in the preequilibrium stage to improve the simulation of complex-particle emission. The coalescence model as described in Refs. [85,86] was included in CEM03.01 and the corresponding coalescence probabilities were adjusted to the available experimental data on the complex-particle yields for the proton and neutron induced reactions [83]. The Kalbach systematics [87] has been also incorporated to describe angular distributions of both preequilibrium nucleons and complex particles at incident energies up to 210 MeV. For the evaporation stage CEM03.01 uses a modification of the code GEM2 by Furihata [71] that considers evaporation of light nuclei up to ^{28}Mg simultaneously with possible emission of nucleons and light clusters ($d, t,{}^3$He, and ^{4}He) solely considered by most of the evaporation models.

The LAQGSM03.01 code differs from CEM03.01 solely by the INC stage. The INC of LAQGSM03.01 is based on the improved version [88,89] of the time-dependent intranuclear cascade model developed initially at JINR, Dubna [85]. It uses the experimental elementary cross sections for energies below 4.5 GeV/nucleon and the calculated ones by the quark-gluon string model [90–93] for higher energies to simulate both the angular and energy distributions of INC particles. In contrast to the earlier versions of the Dubna codes [58,94] and also to CEM03.01 the LAQGSM03.01 code uses a continuous nuclear density distribution, for which there is no a need to consider refraction and reflection of cascade particles inside or on borders of nuclear zones simulated by many other INC codes. It also keeps track on the depletion of the nuclear density during the cascade development (the so-called "trawling effect") that becomes important for incident energies above 5 GeV [58].

VI. COMPARISON OF EXPERIMENTAL DATA WITH CALCULATIONS

The modeling was carried out at 17 energies from 0.1 to 3.5 GeV to produce smooth excitation functions (EF).

The cumulative yields required for comparison with experimental data were calculated by formula (7). The metastable

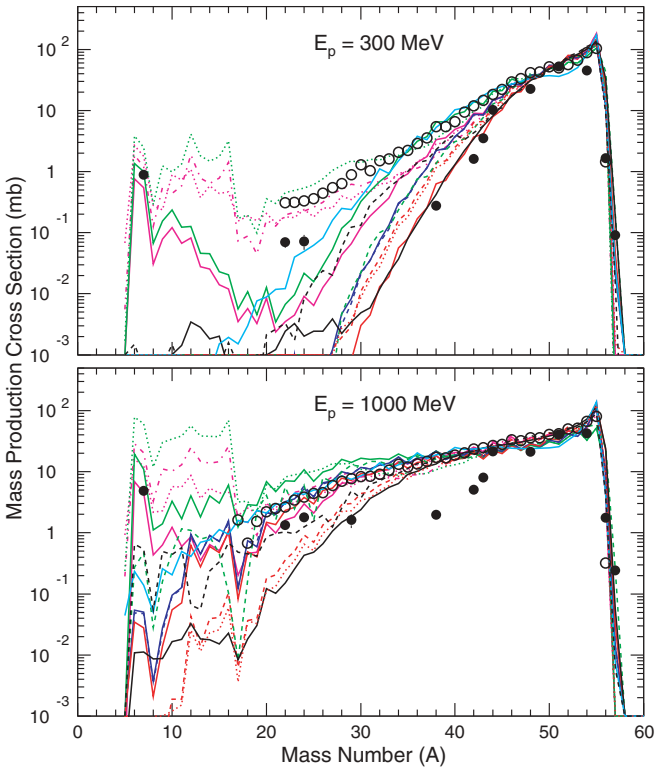

FIG. 8. (Color) Mass distributions of ^{56}Fe(p, x) reaction products measured at ITEP (filled circles) and GSI (open circles) for 300 (top plot) and 1000 MeV (bottom plot) energies as well as simulated by the codes. The codes are designated with the same lines as in Figs. 3–5.

reaction products were not calculated. The calculation-to-experiment comparison results are presented both qualitatively (as plots) and quantitatively [as mean square deviation factors $\langle F \rangle$ calculated by formula (8)].

The measured cross sections were simulated by the all codes described in the previous section.

Each of the above presented codes makes use of its own value for the total reaction cross section. To get a correct comparison among the excitation functions obtained by different codes, the calculated results were renormalized to a single reaction cross section value obtained with the Letaw formula [95].

Figure 8 compares the results of calculating the mass distributions of 300 and 1000 MeV proton-induced reaction products with the experimental data obtained by the inverse kinematics method [43] and with the cumulative yields measured in the present work. Since the cumulative yields correspond to but a fraction of the products, their difference from the GSI data characterizes the contributions from the produced stable isotopes and radioactive isotopes that do not belong to the respective beta-decay chains.

All models give a sufficiently good description of the mass yields of the products close to target nucleus mass ($A >$ 35–40). In the mass range $A < 30$, however, a high-quality description of the observed product nuclide yields is only given by the models that, apart from the conventional evaporation of light nuclei, allow for evaporation of heavy clusters (the CEM and LAQGSM versions). It should be also noted that none of the models gives a good quantitative description of the whole set of experimental data. The CEM03 and LAQGSM models, which are the best to describe the $8 < A < 18$ nuclide yields at 1000 MeV proton energy, predict strong even-odd fluctuations of the yields, which do not seem to affect the experimental data, and give underestimated yields for nuclides with $22 < A < 32$ at 300 MeV proton energy. The experimental data for 1000 MeV proton energy are clearly inclusive of three mass number ranges, namely, $A < 8$, $8 < A < 20$, and $A > 20$. So, our comparison with calculation results produces the impression that different reaction mechanisms dominate in each of the three ranges and, therefore, the qualitative representation of experimental data necessitates a more thorough simulation of each mechanism.

The general regularities of the energy dependence of cumulative yields presented in Figs. 3–5 can be readily accounted for. The reaction products whose mass numbers are only a few unities below the target nucleus (for example, ^{53}Fe, ^{52}Mn, and ^{51}Cr), are produced with sufficiently large cross sections as early as at ∼100 MeV, and their yields decrease with increasing the projectile proton energy. This decrease in the yields is due to production of an ever increasing number of reaction products as the energy rises and, because the total reaction cross section varies but little with increasing energy, the yield of a given nuclide decreases as the total cross section gets distributed over an ever rising number of product nuclides.

The reaction products, whose mass numbers differ from target nucleus by more than a dozen of unities (^{49}Cr and the lighter nuclides) may be produced only starting from a certain higher threshold energy, which is of the order of the mass difference multiplied by 10–15 MeV. Initially, with increasing the energy of bombarding protons, the yields of such nuclides increase and, after that, begin falling in conformity with the above discussed general regularity of decreasing yields as the number of products increases. The threshold energies of the lightest nuclei are sufficiently high, so only the initial stage of the yield increases with rising the projectile proton energy.

However, the Co isotopes, whose charge is a unity above the target nucleus charge, as well as the ^{56}Mn isotope, whose yield increases with proton energy (Fig. 3), should be singled out from the above mentioned regularities. At energies below the π-meson production threshold (∼140 MeV), the ^{57}Co isotope is only produced in the reaction of direct or pre-equilibrium proton capture. This reaction mechanism has been rather well studied for projectile neutrons. The reaction cross section is ∼1 mb for all medium nuclei and decreases with increasing the projectile energy. Above the π-meson production threshold, the ^{57}Co isotope can by produced via the (p, π^0) reaction, whose cross section increases conforming to the general behavioural regularities of threshold reactions.

The ^{56}Co isotope is produced in a direct reaction involving excitation of the analogue states of the daughter nucleus. The cross section of such reactions is sufficiently large (comparable with the integral cross section of inelastic proton scattering reactions) and decreases with increasing the projectile energy in conformity with the general regularities of the cross section

TABLE V. The mean square deviation factors $\langle F \rangle$ for each of the product group combinations and for each energy based on the ITEP experimental data.

Code/model	Product mass (A), proton energy (MeV)												All energies, all products
	300		500		750		1000		1500		2600		
	$A < 30$	$A > 30$	$A < 30$	$A > 30$	$A < 30$	$A > 30$	$A < 30$	$A > 30$	$A < 30$	$A > 30$	$A < 30$	$A > 30$	
MCNPX/INCL	233	5.04	141	3.19	51.5	3.09	38.1	3.08	26.1	3.30	12.1	3.47	7.36
MCNPX/CEM2K	–	2.73	17.2	2.49	21.1	**2.57**	7.83	2.72	4.87	2.88	4.02	3.15	3.64
MCNPX/BERTINI	1035	2.27	19.4	**2.27**	50.5	2.73	13.8	2.85	4.93	3.16	3.35	3.19	4.41
MCNPX/ISABEL	–	4.04	158	2.82	49.1	2.99	17.1	2.62	5.99	2.83	4.02	**2.99**	4.59
LAHET/BERTINI	542	2.29	24.9	**2.26**	6.98	2.66	16.5	3.15	7.34	3.37	5.69	**3.14**	4.09
LAHET/ISABEL	–	2.86	100	2.60	44.6	3.00	15.4	3.43	7.34	3.37	5.69	**3.14**	4.83
CEM03.01	13.0	**1.81**	**1.99**	**1.88**	**1.32**	**1.88**	**1.49**	**1.92**	**1.58**	**2.04**	1.72	3.17	**2.24**
CEM03.G1	**2.82**	2.54	2.35	2.59	**2.42**	2.60	**2.15**	**2.34**	**1.67**	**2.31**	**1.57**	**3.10**	**2.50**
CEM03.S1	**3.35**	**2.20**	3.73	2.32	4.21	2.68	4.94	2.94	6.19	3.25	6.98	4.34	3.33
LAQGSM03.01	45.3	**2.07**	6.98	**1.94**	3.15	**2.02**	2.43	**2.09**	1.98	**2.19**	**1.46**	3.74	**2.89**
LAQGSM03.G1	**2.43**	4.00	**1.85**	2.47	**1.73**	2.76	**1.66**	2.77	**1.50**	2.90	**1.60**	4.22	2.93
LAQGSM03.S1	4.64	2.79	4.35	2.41	3.75	2.67	3.89	2.67	4.17	2.66	3.59	4.13	3.10
CASCADE-2004	4.69	2.70	**1.87**	2.84	12.4	3.13	8.00	3.72	4.55	5.43	3.04	6.48	4.27
LAHETO	–	4.07	108	2.43	22.8	2.83	38.9	3.24	–	–	–	–	5.45
BRIEFF 1.5.4g	208	2.47	12.5	3.00	8.01	3.51	6.41	3.71	5.15	3.89	3.84	3.82	4.74

decrease due to increasing number of reaction products. ^{55}Co belongs to such products, is produced from ^{56}Co after neutron emission, and its cross section obeys the general regularities.

Above the π-meson production threshold, the ^{56}Mn isotope is produced in the ^{56}Fe(p, $p\pi^+$) reaction, whose cross section increases with energy conforming to the high threshold reaction behavioral regularities. Below the meson production threshold, ^{56}Mn can only be produced in the neutron-induced ^{56}Fe(n, p) reaction. Such neutrons may be generated due to induced activity in the target chamber. The background effects of this type may be expected to define the difference in the ^{56}Mn cumulative yields in the given measurements and in inverse kinematics measurements that are free of the neutron background effects.

The general regularities of the energy dependences of reaction product yields discussed above have been corroborated by calculations made by all the models presented in Figs. 3–5. At the same time, the quantitative results are contingent upon a particular model used, so the observed discrepancies follow directly from the differences in the respective models.

To get a better understanding of how the various codes simulate the experimental data, all the reaction products were divided into two groups of the spallation ($A > 30$) and fragmentation ($A < 30$) reaction products, respectively. Table V presents the mean square deviation factors $\langle F \rangle$ for each of the product group combinations and for each energy based on the ITEP experimental data. The energies used in comparisons correspond to the experiment. Table VI presents analogous results based on the GSI measurements [after convolution of independent yields into cumulative ones using formula (10)]. In Tables V and VI, the bold numerals designate three best codes, while the underlined numerals indicate three worst codes. Figure 9 demonstrates the predictive power of each

TABLE VI. The mean square deviation factors $\langle F \rangle$ for each of the product group combinations and for each energy based on the GSI experimental data.

Code/model	Product mass (A), proton energy (MeV)										All energies, all products
	300		500		750		1000		1500		
	$A < 30$	$A > 30$	$A < 30$	$A > 30$	$A < 30$	$A > 30$	$A < 30$	$A > 30$	$A < 30$	$A > 30$	
MCNPX/INCL	153	5.85	52.0	3.30	15.8	3.10	10.2	2.25	6.63	3.27	6.06
MCNPX/CEM2K	1598	3.09	17.7	2.70	3.96	2.66	3.54	1.96	3.88	2.69	3.59
MCNPX/BERTINI	534	2.45	18.8	**1.66**	3.48	**1.54**	2.80	**1.70**	3.00	**1.95**	2.75
MCNPX/ISABEL	–	4.76	124	2.81	39.3	2.57	3.54	**1.79**	3.42	2.69	4.21
LAHET/BERTINI	1369	2.78	22.7	**1.82**	5.75	**1.66**	4.67	2.07	5.44	2.18	3.80
LAHET/ISABEL	1224	2.90	91.4	2.52	35.5	2.23	13.7	2.06	5.44	2.18	5.29
CEM03.01	27.6	**1.86**	**2.20**	2.08	**1.58**	2.09	**1.69**	**1.58**	**1.59**	2.18	**2.35**
CEM03.G1	**3.49**	2.65	3.23	3.11	3.36	2.95	2.61	2.15	1.77	2.52	2.72
CEM03.S1	5.42	2.68	4.91	2.62	4.07	2.70	4.83	2.51	5.50	3.28	3.10
LAQGSM03.01	97.9	**1.93**	7.59	**1.89**	2.66	1.93	2.06	1.90	**1.69**	**1.61**	2.82
LAQGSM03.G1	**4.22**	**2.26**	**1.97**	2.64	**1.77**	2.85	**1.53**	2.76	**1.48**	2.46	**2.52**
LAQGSM03.S1	13.4	3.16	5.69	2.54	3.76	2.44	4.15	2.35	4.17	2.04	2.97
CASCADE-2004	**4.90**	2.65	**1.54**	**2.95**	**1.69**	2.27	**1.94**	2.04	1.76	2.24	**2.41**
LAHETO	–	3.65	107	2.36	20.2	2.67	34.7	2.72	–	–	5.03
BRIEFF 1.5.4g	42.2	3.38	4.86	2.19	3.18	1.96	2.99	1.89	2.62	**1.81**	2.58

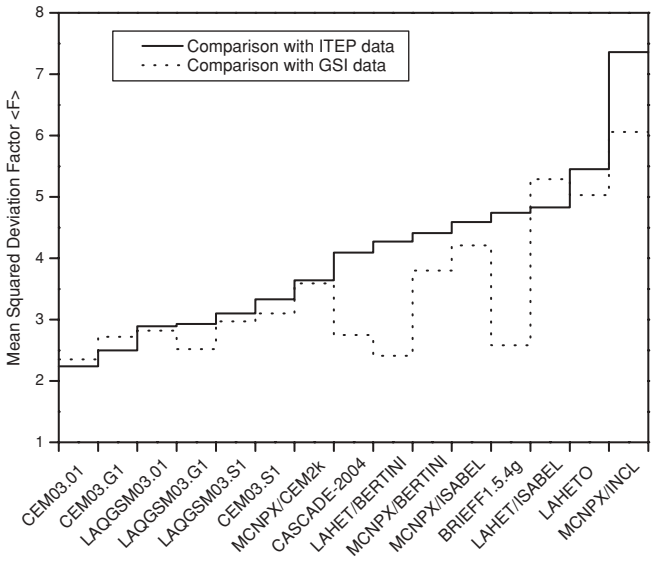

FIG. 9. The predictive power of each code (the mean square deviation factors for all energies and all products).

code (the mean square deviation factors for all energies and all products).

VII. CONCLUSION

The work presents results of measuring the production cross sections of radioactive nuclides from 300, 500, 750, 1000, 1500, and 2600 MeV protons irradiating ^{56}Fe. In total, 221 independent and cumulative yields of radioactive nuclei of halftimes from 6.6 min to 312 d have been measured. The yields obtained have been compared with results of earlier activation measurements of the cumulative yields of the products of proton interactions with the said Fe isotope and were also compared with the inverse kinematics measurements of the independent product yields from the up to 1500 MeV proton-induced reactions. Most of the data obtained here are in a good agreement with the inverse kinematics results and disprove the results of some earlier activation measurements that were quite different from the inverse kinematics measurements.

The total experimental data array has been compared with the results by 15 different models. The main discrepancies between different model versions and experimental data have been discussed in brief. The most significant calculation-to-experiment differences are observed in the yields of the $A < 30$ light nuclei, indicating that further improvements in nuclear reaction models are needed, and pointing out as well to a necessity of more complete experimental measurements of such reaction products.

ACKNOWLEDGMENTS

We thank Drs. S. Leray, A. Kelić, K.-H. Schmidt, and A. J. Sierk for useful discussions of our results and several valuable suggestions on their presentation in the present paper. This work has been carried out under the EC-supported ISTC Project No. 3226. The work has also been supported by the Federal Atomic Energy Agency of Russia and, in part, by the U.S. Department of Energy at Los Alamos National Laboratory under Contract DE-AC52-06NA25396.

[1] *Proceedings of the International Conference on Accelerator-Driven Transmutation Technologies and Applications*, Las Vegas, 1994, edited by E. D. Arthur, A. Rodrigues, and S. O. Schriber (AIP, Woodbury, NY, 1995).

[2] Experimental Nuclear Reaction Data (EXFOR) database, http://www-nds.iaea.org/exfor/exfor00.htm Accession Nos. O0276*, O0277*, A0344*, O0078016, A0100007.

[3] Experimental Nuclear Reaction Data (EXFOR) database, http://www-nds.iaea.org/exfor/exfor00.htm Accession No. O0284*.

[4] Experimental Nuclear Reaction Data (EXFOR) database, http://www-nds.iaea.org/exfor/exfor00.htm Accession Nos. O0729013, O0728016.

[5] Experimental Nuclear Reaction Data (EXFOR) database, http://www-nds.iaea.org/exfor/exfor00.htm Accession Nos. A0479*, O0281*, A0479*, A0408005, O0080005, A0516002, C0235*, C0226005, B0085024, O0095008, O0085022, O0077012, O0073008, O0094010, O0299002, O0299*, A0501054, O0159003, T0131002, C0555008, O0104004, C0329002, C0269016, C0272003, C0253026, O0339025, O0046004, O0044026, O0584007, O0410005, O0088007, C0277008.

[6] W. R. Webber, J. C. Kish, J. M. Rockstroh *et al*., Astrophys. J. **508**, 949 (1998).

[7] C. Villagrasa-Canton, A. Boudard, J.-E. Ducret, P. Napolitani, K. H. Schmidt, A. S. Botvina, F. Rejmund, L. Tassan-Got, C. Villagrasa, Phys. Rev. C **75**, 044603 (2007); Carmen Villagrasa-Canton, Ph.D. thesis, Université Paris XI, France, September 2004, http://www-w2k.gsi.de/charms/theses.htm; E. Le Gentil, M. Bömer, A. Lafriakh *et al*., Nucl. Instrum. Methods Phys. Res. A **562**, 743 (2006) ; E. Le Gentil, T. Aumann, C. O. Bacri *et al*., Phys. Rev. Lett. **100**, 022701 (2008).

[8] P. Napolitani, K.-H. Schmidt, A. S. Botvina *et al*., Phys. Rev. C **70**, 054607 (2004); Paolo Napolitani, Ph.D. thesis, Université Paris XI, France, September 2004, http://www-w2k.gsi.de/charms/theses.htm.

[9] Yu. E. Titarenko, O. V. Shvedov, M. M. Igumnov *et al*., Nucl. Instrum. Methods Phys. Res. A **414**, 73 (1998).

[10] Yu. E. Titarenko, O. V. Shvedov, V. F. Batyaev *et al*., Phys. Rev. C **65**, 064610 (2002).

[11] Yu. E. Titarenko, V. F. Batyaev, E. I. Karpikhin *et al*., Final Project Technical Report of ISTC 839B-99 of February 2001, IAEA, Nuclear Data Section, Wagramer Strasse 5, A-1400 Vienna, NDC(CCP)-434, September 2002, http://www-nds.iaea.org/reports/indc-ccp-434.pdf.

[12] Yu. E. Titarenko, V. F. Batyaev, V. M. Zhivun *et al*., LANL Report LA-UR-03-3403; arXiv:nucl-ex/0305026; Proceedings of the AccApp'03 Embedded Topical Meeting "Accelerator Applications in a Nuclear Renaissance," San Diego, California, June 1–5, 2003 (ANS, La Grange Park, IL, 2004), pp. 59–66.

[13] Yu. E. Titarenko, V. F. Batyaev, E. I. Karpikhin *et al*., Final Technical Report on the ISTC Project No.

2002, http://www.nea.fr/html/science/egsaatif/ISTC2002-final-report.pdf.
[14] G. F. Steyn *et al.*, Appl. Radiat. Isot. **41**, 315 (1990).
[15] J. Tobailem and C. H. de Lassus, CEA-N-1466(5) (1981).
[16] J. Tobailem and C. H. de Lassus, CEA-N-1466(1) (1975).
[17] Experimental Nuclear Reaction Data (EXFOR) database, http://www-nds.iaea.org/exfor/exfor00.htm Accession Nos. C0259*, B0076*, C0250*, D4101*, D0128*, C0394*, B0095*, P0016*, B0073*, O0449*, O0350*, O0501*, A0151*, D0053*, A0178*, D0028*, A0340*, A0445*, A0478*, O0282*, A0518*, A0519*, C0196*, A0581*, C0461*.
[18] R. R. Kinsey *et al.*, in *Proceedings of the Ninth International Symposium on Capture Gamma-Ray Spectroscopy and Related Topics*, Budapest, Hungary, 1996, edited by G. L. Molnar, T. Belgya, and Z. S. Revay (Springer Verlag, Heidelberg, 1997); http://www.fysik.lu.se/nucleardata/cdrom/pcnudat.htm.
[19] R. B. Firestone, in *Tables of Isotopes*, 8th ed. 1998 Update (with CD ROM), edited by S. Y. Frank Chu (CD-ROM editor) and C. M. Baglin (Wiley Interscience, New York, 1996).
[20] J. K. Tuli, A Manual for Preparation of Data Sets, BNL-NCS-51655-01/02-Rev, February 2001, http://ie.lbl.gov/databases/ENSDF-Manual.pdf. ENSDF database is available at http://ie.lbl.gov/databases/ENSDFdata. exe.
[21] E. Storm and H. I. Israel, Nucl. Data Tables A **7**, 565 (1970).
[22] J. Tobailem and C. H. Lassus St-Genies, Note CEA-N-1466(3), Saclay, 1075.
[23] J. Tobailem, Sections Efficaces des Reactions Nucleaires Indutes par Protons, Deuterons, Particles Alphas. V. Silicium, Note CEA-N-1466(5), Saclay, 1981.
[24] R. E. Prael and H. Lichtenstein, User Guide to LCS: The LAHET Code System, LA-UR-89-3014, Los Alamos (1989).
[25] H. W. Bertini, Phys. Rev. **188**, 1711 (1969).
[26] Y. Yariv and Z. Fraenkel, Phys. Rev. C **20**, 2227 (1979).
[27] J. S. Hendricks, G. W. McKinney, L. S. Waters *et al.*, MCNPX EXTENSIONS Version 2.5.0, LANL Report LA-UR-05-2675, Los Alamos (April 2005); http://mcnpx.lanl.gov/.
[28] S. G. Mashnik and A. J. Sierk, CEM2K—Recent Developments in CEM, *Proceedings of the 2000 ANS/ENS International Meeting, Embedded Topical Meeting Nuclear Applications of Accelerator Technology (AccApp00)*, November 12–16, 2000, Washington, DC (USA) (American Nuclear Society, La Grange Park, IL, 2001), pp. 328–341; arXiv:nucl-th/0011064.
[29] A. Boudard, J. Cugnon, S. Leray, and C. Volant, Phys. Rev. C **66**, 044615 (2002).
[30] J.-J. Gaimard and K.-H. Schmidt, Nucl. Phys. **A531**, 709 (1991); A. R. Junghans, M. de Jong, H.-G. Clerc *et al.*, *ibid.* **A629**, 635 (1998).
[31] H. Kumawat and V. S. Barashenkov, Eur. Phys. J. A **26**, 61 (2005); Harphool Kumawat, Ph.D. thesis [in Russian], JINR, Dubna, Russia (2004).
[32] A. V. Ignatyuk, N. T. Kulagin, V. P. Lunev *et al.*, in *Proceedings of the International Conference on Nuclear Data for Science and Technology (ND2004)*, September 26–October 1, 2004, Santa Fe, NM, USA, edited by R. C. Haight, M. B. Chadwick, T. Kawano, and P. Talou [AIP Conf. Proc. **769**, 1307 (2005)].
[33] H. Duarte, Phys. Rev. C **75**, 024611 (2007).
[34] H. Duarte, Proceedings of the ND2007 International Conference on Nuclear Data for Science and Technology, Nice, France, April 22–27 (2007).
[35] S. G. Mashnik, K. K. Gudima, A. J. Sierk *et al.*, in [32] [(AIP Conf. Proc. **769**, 1188 (2005)]; arXiv:nucl-th/0502019.
[36] S. G. Mashnik, K. K. Gudima, M. I. Baznat *et al.*, LANL Report LA-UR-06-1764, Los Alamos (2006); LANL Report LA-UR-06-1955, Los Alamos (2006); arXiv:nucl-th/0603046.
[37] T. W. Armstrong and K. C. Chandler, Nucl. Sci. Eng. **49**, 110 (1972), and references therein; Radiation Shielding Information Center, "HETC Monte Carlo High-Energy Nucleon-Meson Transport Code," Report CCC-178, Oak Ridge National Laboratory (August 1977).
[38] R. E. Prael and M. Bozoian, Los Alamos National Laboratory Report LA-UR-88-3238 (September 1988).
[39] E. Fermi, Prog. Theor. Phys. **5**, 570 (1950).
[40] J. V. Lepore and R. N. Stuart, Phys. Rev. **94**, 1724 (1954).
[41] A. P. Zhdanov and P. I. Fedorov, Zh. Eksp. Teor. Fiz. **45**, 455 (1963) [Sov. Phys. JETP **18**, 313 (1964)].
[42] E. Gradsztajn, F. Yiou, R. Klapisch *et al.*, Phys. Rev. Lett. **14**, 436 (1965).
[43] T. S. Subramanian, J. L. Romero, F. P. Brady *et al.*, Phys. Rev. C **28**, 521 (1983).
[44] F. Atchison, in *Proceedings of the Meeting on Targets for Neutron Beam Spallation Source*, Jülich, June 11–12, 1979, edited by G. S. Bauer, Jul-Conf-34 (Kernforschungsanlage Jülich GmbH, Germany 1980), pp. 17–46; *Proceedings of a Specialists' Meeting*, May 30–June 1, 1994, Issy-Les-Moulineaux, France (OECD, Paris, France, 1994) pp. 199–218; Nucl. Instrum. Methods Phys. Res. B **259**, 909 (2007).
[45] J. Barish *et al.*, ORNL/TM-7882, Oak Ridge National Laboratory (1981); F. S. Alsmiller, R. G. Alsmiller, Jr., T. A. Gabriel *et al.*, Nucl. Sci. Eng. **79**, 147 (1981).
[46] P. Fong, *Statistical Theory of Nuclear Fission* (Gorgon and Breach Science Publishers, New York, 1969).
[47] L. S. Waters, G. W. McKinney, J. W. Durkee *et al.*, *Proceedings of the Hadronic Shower Simulation Workshop (HSSW06), FNAL*, Batavia, IL, USA, September 6–8, 2006 [AIP Conf. Proc. **896**, 81 (2007)].
[48] K. K. Gudima, S. G. Mashnik, and V. D. Toneev, Nucl. Phys. **A401**, 329 (1983).
[49] S. G. Mashnik and A. J. Sierk, in *Proceedings of the Fourth International Workshop on Simulating Accelerator Radiation Environments* (SARE4), Knoxville, TN, 1998, edited by T. A. Gabriel (ORNL, 1999), p. 29; arXiv:nucl-th/9812069.
[50] S. G. Mashnik, User manual for the code CEM95, JINR, Dubna, 1995; OECD Nuclear Energy Agency Data Bank, Paris, France, 1995; http://www.nea.fr/abs/html/iaea1247.html; RSIC-PSR-357, Oak Ridge, 1995.
[51] J. Cugnon, T. Mizutani, and J. Vandermeulen, Nucl. Phys. **A352**, 505 (1981).
[52] J. Cugnon, P. Jasselette, and J. Vandermeulen, Nucl. Phys. **A470**, 558 (1987).
[53] J. Cugnon, Nucl. Phys. **A462**, 751 (1987).
[54] J. Cugnon and M.-C. Lemaire, Nucl. Phys. **A489**, 781 (1988).
[55] L. Pienkowski, H. G. Bohlen, J. Cugnon *et al.*, Phys. Lett. **B336**, 147 (1994).
[56] J. Cugnon, Th. Aoust, P. Henrotte *et al.*, in [32] [AIP Conf. Proc. **769**, 1172 (2005)].
[57] Le van Ngok, L. G. Levchuk, Zh. Zh. Musulmanbekov *et al.*, JINR Communication P2-85-173, Dubna (1985).
[58] V. S. Barashenkov and V. D. Toneev, *Interaction of high energy particles and nuclei with atomic nuclei* (in Russian) (Atomizdat, Moscow, 1972).
[59] V. S. Barashenkov, A. S. Iljinov, N. M. Sobolevsky *et al.*, Usp. Fiz. Nauk **109**, 91 (1973) [Sov. Phys. Usp. **16**, 31 (1973)].

[60] V. S. Barashenkov, Comput. Phys. Commun. **126**, 28 (2000).
[61] V. D. Toneev and K. K. Gudima, Nucl. Phys. **A400**, 173 (1983).
[62] K. K. Gudima, G. A. Ososkov, and V. D. Toneev, Yad. Fiz. **21**, 260 (1975) [Sov. J. Nucl. Phys. **21**, 138 (1975)].
[63] S. G. Mashnik and V. D. Toneev, JINR Communication P4-8417, Dubna (1974).
[64] I. Dostrovsky, Z. Frankel, and G. Friedlander, Phys. Rev. **116**, 683 (1959).
[65] H. Kumawat, D. Dutta, V. Mantha *et al*., Nucl. Instrum. Methods Phys. Res. B **266**, 604 (2008).
[66] A. V. Ignatyuk, G. N. Smirenkin, and A. S. Tishin, Yad. Fiz. **21**, 485 (1975) [Sov. J. Nucl. Phys. **21**, 255 (1975)]; A. V. Ignatyuk, M. G. Itkis, V. N. Okolovich *et al*., *ibid*. **21**, 1185 (1975) [Sov. J. Nucl. Phys. **21**, 612 (1975)].
[67] A. V. Ignatyuk, Yad. Fiz. **21**, 20 (1975) [Sov. J. Nucl. Phys. **21**, 10 (1975)]; I. Blokhin, A. V. Ignatyuk, and Yu. N. Shubin, *ibid*. **48**, 371 (1988) [Sov. J. Nucl. Phys. **48**, 232 (1988)]; A. V. Ignatyuk, J. L. Weil, S. Raman, and S. Kahane, Phys. Rev. C **47**, 1504 (1993).
[68] V. F. Weisskopf and D. H. Ewing, Phys. Rev. **57**, 472 (1940).
[69] H. Duarte, Proceedings of 3rd International Conference on Accelerator Driven Transmutation Technologies and Applications, Praha, 7–11 June 1999, Czech Republic, paper Mo-O-C17 on the webpage http://www.fjfi.cvut.cz/con%5Fadtt99/.
[70] H. Duarte, in *Proceedings of the International Workshop on Nuclear Data for the Transmutation of Nuclear Waste (TRAMU)*, edited by A. Kelic and K.-H. Schmidt, September 1–5 (GSI-Darmstadt, Germany, 2003), ISBN 3-00-012276-1, http://www-w2k.gsi.de/tramu/Proceedings.htm; *Proceedings of the 10th International Conference on Nuclear Reaction Mechanisms, Varenna, Italy, June 9–13, 2003*, edited by E. Gadioli, pp. 607–616.
[71] S. Furihata, Nucl. Instrum. Methods Phys. Res. B **171**, 252 (2000); Ph.D. thesis, Tohoku University, Japan, 2003, and references therein.
[72] J. P. Bondorf, A. S. Botvina, A. S. Iljinov *et al*., Phys. Rep. **257**, 133 (1995).
[73] A. S. Botvina, A. S. Iljinov, I. N. Mishustin *et al*., Nucl. Phys. **A475**, 663 (1987).
[74] A. S. Botvina, K. K. Gudima, A. S. Iljinov *et al*., Yad. Fiz. **57**, 667 (1994) [Phys. At. Nucl. **57**, 628 (1994)].
[75] A. S. Botvina, A. S. Iljinov, and I. N. Mishustin, Nucl. Phys. **A507**, 649 (1990).
[76] A. S. Botvina, A. S. Iljinov, and I. N. Mishustin, Yad. Fiz. **42**, 1127 (1985) [Sov. J. Nucl. Phys. **42**, 712 (1985)].
[77] R. J. Charity, M. A. McMahan, G. J. Wozniak *et al*., Nucl. Phys. **A483**, 371 (1988).
[78] L. G. Sobotka, M. A. McMahan, R. J. McDonald *et al*., Phys. Rev. Lett. **53**, 2004 (1984).
[79] R. J. Charity, D. R. Bowman, Z. H. Liu *et al*., Nucl. Phys. **A476**, 516 (1988).
[80] R. J. Charity, Phys. Rev. C **58**, 1073 (1998).
[81] R. J. Charity, L. G. Sobotka, J. Cibor *et al*., Phys. Rev. C **63**, 024611 (2001); http://www.chemistry.wustl.edu/∼rc/gemini/.
[82] L. G. Moretto, Nucl. Phys. **A247**, 211 (1975).
[83] S. G. Mashnik, K. K. Gudima, A. J. Sierk *et al*., LANL Report LA-UR-05-7321, Los Alamos, 2005; RSICC code package PSR-532, http://www-rsicc.ornl.gov/codes/psr/psr5/psr-532.html.
[84] S. G. Mashnik, M. I. Baznat, K. K. Gudima *et al*., J. Nucl. Radiochem. Sci. **6**, A1 (2005); arXiv:nucl-th/0503061.
[85] V. D. Toneev and K. K. Gudima, Nucl. Phys. **A400**, 173c (1983).
[86] K. K. Gudima, G. Röpke, H. Schulz *et al*., JINR Communication JINR-E2-83-101, Dubna (1983); H. Schulz, G. Röpke, K. K. Gudima *et al*., Phys. Lett. **B124**, 458 (1983).
[87] C. Kalbach, Phys. Rev. C **37**, 2350 (1988).
[88] K. K. Gudima and S. G. Mashnik, in *Proceedings of the 11th International Conference on Nuclear Reaction Mechanisms, Varenna, Italy, June 12–16, 2006*, edited by E. Gadioli, pp. 525–534; arXiv:nucl-th/0607007.
[89] S. G. Mashnik, K. K. Gudima, M. I. Baznat *et al*., LANL Report LA-UR-05-2686, Los Alamos (2005).
[90] N. S. Amelin, K. K. Gudima, and V. D. Toneev, Sov. J. Nucl. Phys. **51**, 327 (1990) [Yad. Fiz. **51**, 512 (1990)]; **51**, 1093 (1990) [Yad. Fiz. **51**, 1730 (1990)]; **52**, 1722 (1990) [Yad. Fiz. **52**, 272 (1990)], and references therein.
[91] N. S. Amelin, JINR Communication JINR-86-802, Dubna (1986).
[92] A. B. Kaidalov, Sov. J. Nucl. Phys. **45**, 902 (1987) [Yad. Fiz. **45**, 1452 (1987)].
[93] N. S. Amelin, V. S. Barashenkov, and N. V. Slavin, Sov. J. Nucl. Phys. **40**, 991 (1984) [Yad. Fiz. **40**, 1560 (1984)]; N. S. Amelin and A. I. Ostrovidov, *ibid*. **50**, 302 (1989) [Yad. Fiz. **50**, 486 (1989)].
[94] V. S. Barashenkov, K. K. Gudima, and V. D. Toneev, JINR Communication P2-4066, Dubna (1968); Acta Physica Pol. **36**, 415 (1969); K. K. Gudima, A. S. Iljinov, and V. D. Toneev, Communication JINR P2-4661, Dubna (1969).
[95] J. R. Letaw, R. Silberberg, and C. H. Tsao, Astrophys. J., Suppl. **51**, 271 (1983).